Single Molecule Photon Counting Statistics for Quantum Mechanical Chromophore Dynamics†

Golan Bel, Yujun Zheng,‡ and Frank L. H. Brown*

Department of Chemistry and Biochemistry, University of California, Santa Barbara, California 93106-9510

Received: April 16, 2006; In Final Form: July 27, 2006

We extend the generating function technique for calculation of single molecule photon emission statistics (Zheng, Y.; Brown, F. L. H. *Phys. Rev. Lett.* **2003**, *90*, 238305) to systems governed by multi-level quantum dynamics. This opens up the possibility to study phenomena that are outside the realm of purely stochastic and mixed quantum-stochastic models. In particular, the present methodology allows for calculation of photon statistics that are spectrally resolved and subject to quantum coherence. Several model calculations illustrate the generality of the technique and highlight quantitative and qualitative differences between quantum mechanical models and related stochastic approximations when they arise. Calculations suggest that studying photon statistics as a function of photon frequency has the potential to reveal more about system dynamics than the usual broadband detection schemes.

I. Introduction

Single molecule spectroscopy (SMS) has become a versatile and powerful tool for the study of condensed phase systems in chemistry, physics, and biology.[1−12] Unfortunately, the very qualities that make SMS such a powerful technique have also led to significant theoretical challenges in describing experimental data. The ultra-microscopic nature of the physical systems under study leads to randomness in the behavior of experimental signals due both to thermal agitation of the photoactive portion of the system and to the inherent randomness of the spontaneous emission process itself. While SMS has been hailed for its ability to probe these fluctuations directly, it remains difficult to extract physical pictures for molecular dynamics based solely on SMS data streams. Some of this difficulty is likely fundamental (current SMS experiments may not collect sufficient data to allow for direct inversion to molecular dynamics), but even if SMS data were sufficient to differentiate between all viable physical hypotheses, it remains an open question as to the best means to simulate such models to allow for comparison with experiment. Indeed, much effort has been expended on the theory of interpreting/modeling SMS trajectories, particularly in the context of stochastic models for chromophore dynamics.[12−30] Stochastic models, though certainly illustrative and powerful, ultimately face certain limitations in the modeling of phenomena that are inherently quantum mechanical, such as spectroscopy. Quantum coherence cannot be captured, quantization of nuclear eigenstates is not naturally formulated within a stochastic scheme, and the parameters of stochastic models are often difficult to equate with their microscopic origins. As the following work will show, even stochastic models systematically derived from underlying quantum considerations can lead to quantitative and qualitative differences from fully quantum calculations. As expected, these deviations are small for two-level chromophores when coupling between the chromophore and environment is very weak but can become substantial in other regimes and for more realistic chromophore models.

Until recently, Monte Carlo Wave Function simulations (MCWF)[31] and related techniques provided the only fully satisfactory route to theoretical calculation of single molecule photon counting observables[32] including quantum mechanical effects. A few other studies have touched on specific aspects of quantum dynamics applicable to SMS[24,27,33−35] but without complete generality. Recent work by us[36−39] and others[40−44] has established generating function techniques as a general means for calculating statistical quantities of single molecule photon counting experiments. The only fundamental limitations to this approach are that you must consider the spontaneous emission of photons to be governed by rate processes and the directly calculated quantities are statistical moments of the number of photons emitted.[36,37,41]

The bulk of previous work with the generating function approach has focused on two-level chromophores with stochastic modulation by the environment, however the method is equally applicable to multi-state quantum systems. The extension to multi-state quantum systems was suggested by us[37] and formally carried out by Mukamel.[41] Sanda and Mukamel[44] have recently used the generating function approach to derive formal perturbative expressions (in the applied field strength) for low-order photon counting moments. Though interesting from a theoretical standpoint, the derived expressions are complex enough that implementation will be impossible for all but the simplest model systems (second-order moments require solution of a six point quantum correlation function, higher moments need larger correlations). As a numerical technique, the generating function approach has promise to study varied systems without limitation to low field strengths.

The present paper considers several model systems to demonstrate the use of the generating function approach as a numerical tool for predicting SMS photon counting observables. In addition to calculation of photon counting moments for broadband detection schemes, as has been considered previously, we also calculate emission statistics for photons specific to particular

† Part of the special issue "Robert J. Silbey Festschrift".

* To whom correspondence should be addressed. E-mail: flbrown@chem.ucsb.edu.

‡ Present address: School of Physics and Microelectronics, Shandong University, Jinan 250100, Shandong, China.

10.1021/jp062345v CCC: $33.50
Published on Web 09/21/2006

molecular transitions and degenerate sets of transitions. For systems where vibrational structure is well resolved compared with natural line widths, this is equivalent to the calculation of spectrally resolved emission statistics. From a conceptual and numerical standpoint, these calculations are no more difficult than broadband detection calculations. The simulations we have carried out suggest that significantly more information stands to be learned from photon counting experiments when photon statistics are broken down by color.

This paper is organized as follows. Section II presents the underlying theory and notation necessary to introduce our calculations. Although there are many details to be considered here, the conceptual framework for calculating photon statistics in the many-level case is no more complex than that for two-level chromophores. Given the reduced Liouvillian operator for density matrix dynamics of the chromophore system, calculation of the generating function for photon number and/or low-order statistical moments is immediate. Most of section II is dedicated to describing the Liouvillian operator itself, not the extension of this matrix to calculation of experimental observables. Sections III and IV present numerical calculations for chromophores coupled to a two-level system and a harmonic vibrational coordinate. Many different regimes are considered, both to display the flexibility of the present formulation in numerical calculations and to highlight differences between fully quantum calculations and commonly employed stochastic approximations. In section V, we conclude.

II. Theoretical Background

A. General Considerations for Chromophore Dynamics. The picture we present is the natural extension of the optical Bloch equations to multi-level quantum systems in a condensed phase. Our methodology has been adopted both to make connection with our previous work on two-level chromophores[36−38] and because the necessary theoretical/computational tools for chromophore dynamics are well established in the literature.

We imagine a single chromophore in a condensed phase environment driven by an external laser field. It is assumed that the field is strong enough to warrant a classical treatment of this perturbation so that dynamics, in the absence of any other system−field interactions, would be dictated by

$$\dot{\rho}(t) = -\frac{i}{\hbar}[\hat{H}^{\mathrm{sys}},\rho] + \frac{i}{\hbar}\boldsymbol{E}(t)\cdot[\hat{\boldsymbol{\mu}},\rho] \tag{1}$$

In the above equation, $\hat{H}^{\mathrm{sys}}$ is the Hamiltonian for the unperturbed chromophore−environment system, $\hat{\boldsymbol{\mu}}$ is the electric dipole moment for this system, and $\boldsymbol{E}(t)$ is the classical applied laser field. $\rho(t)$ specifies the density matrix for the molecule only. This evolution assumes the radiation is of sufficiently long wavelength (and the chromophore sufficiently localized) to allow the dipole approximation.

What the above dynamics neglects is the relaxation of the driven molecular system. The coupling between system and the quantum radiation field provides a route for this relaxation to occur: the spontaneous emission of photons. It is these photons that are registered in SMS experiments, and hence, inclusion of the spontaneous emission process is absolutely essential. Within the standard approximations, the quantum radiation field is integrated over to provide rate constants for emission of photons between various molecular transitions.[45,46] This leads to a master equation approach for incorporating emission events as pure rate processes. The rate for spontaneous emission of a photon, causing a jump from system eigenstate i to eigenstate j, is calculated by the application of Fermi's golden rule (using the coupling between the system and quantum radiation field as the perturbation)

$$\Gamma_{ij} = \frac{\omega_{ij}{}^3 \boldsymbol{D}_{ij}{}^2}{3\pi\epsilon\hbar c^3} \tag{2}$$

$$\boldsymbol{D}_{ij} = \langle i|\hat{\boldsymbol{\mu}}|j\rangle$$

The collection of constants appearing in this expression have their usual meanings (ϵ is the permittivity, $\hbar$ is Planck's constant divided by 2π, and c is the speed of light), but we will not be concerned with them in this work. What is important to us is the dependence on the transition dipole moment $\boldsymbol{D}_{ij}$, which serves to mediate relative rates of emission for different chromophore transitions. In principle, energy splittings (ω_{ij}) impact the rates as well, but we shall be concerned with electronic transitions where differences in this quantity between various allowed transitions are much smaller than the splitting itself. In this limit, we expect inconsequential variations on the basis of energy differences.

Perturbation theory applied to the entire system density matrix evolution (as opposed to just a single rate calculation) additionally tells us that the population lost from state i, via Γ_{ij} decay, ends up in state j. Also, it specifies that the $i \rightarrow j$ transition causes all associated coherences (ρ_{ik}, ρ_{ki}) to decay at the rate of $\Gamma_{ij}/2$. The net effect of all spontaneous emission processes in the system is the additive contribution of these three effects (loss of population from state i, gain in population of state j, and loss of coherence for all allowed $i \rightarrow j$ transitions.) We neglect radiative level shifts in the system states and ignore all other couplings (virtual photon transitions) caused by the presence of the quantum radiation field. These other couplings are unimportant when system energy levels are nondegenerate as the implied perturbations are nonsecular.[45,46] The nondegeneracy condition is met by the systems studied in this work.

Keeping those contributions specified in the last two paragraphs implies that we supplement our chromophore equations of motion with non-Hamiltonian evolution terms corresponding to spontaneous emission. The form of this augmentation is most transparent in the basis of $\hat{H}^{\mathrm{sys}}$ eigenstates. Rewriting eq 1 in this form yields (The summation convention over repeated density matrix labels is assumed throughout this work.)

$$\dot{\rho}_{ij}(t) = \mathbb{L}^{\mathrm{sys}}_{ij;kl}\rho_{kl} + \mathbb{L}^{E}_{ij;kl}(t)\rho_{kl} + \mathbb{L}^{\Gamma}_{ij;kl}\rho_{kl} \tag{3}$$

Here, $\mathbb{L}^{\mathrm{sys}}$ and $\mathbb{L}^{E}(t)$ are Liouville superoperators (matrices) corresponding to the commutator expressions in eq 1.[47] Note that our definition incorporates the factor $-i/\hbar$ within $\mathbb{L}^{\mathrm{sys}}$ and $\mathbb{L}^{E}(t)$. $\mathbb{L}^{\Gamma}$ is the matrix effecting spontaneous emission processes. The elements of this matrix are provided by the arguments of the preceding paragraphs ($i \neq j$ assumed in the following)

$$\mathbb{L}^{\Gamma}_{ii;ii} = -\sum_{k\neq i}\Gamma_{ik}$$

$$\mathbb{L}^{\Gamma}_{jj;ii} = \Gamma_{ij}$$

$$\mathbb{L}^{\Gamma}_{ij;ij} = -\frac{1}{2}\left(\sum_{k\neq i}\Gamma_{ik} + \sum_{k\neq j}\Gamma_{jk}\right) \tag{4}$$

with all other elements being zero.

In what follows, it will be convenient to partition the matrix $\mathbb{L}^{\Gamma}$ into its positive and negative pieces, so that

$$\mathbb{L}^{\Gamma} = \mathbb{L}^{+\Gamma} + \mathbb{L}^{-\Gamma} \tag{5}$$

with $\mathbb{L}^{+\Gamma}$ consisting of the terms specified by the second line of eq 4 and $\mathbb{L}^{-\Gamma}$ comprised of the remaining terms from the first and third lines.

One final important point is that while eq 3 provides effective dynamics for the system with implications of field fluctuations handled implicitly, this dynamic will still be far too complicated for exact practical treatment when the system of interest is composed of a chromophore embedded in a condensed phase. The problem is simply one of a complex dynamic associated with a quantum mechanical many-body system. When it is possible to make some effective separation between the relevant part of the system and a weakly coupled (and fast) bath, this problem can be overcome in exactly the same method employed to remove the radiative field from explicit consideration. Writing

$$\hat{H}^{\mathrm{sys}} = \hat{H}^{\mathrm{ch}} + \hat{H}^{\mathrm{b}} + \hat{V} \tag{6}$$

for a "system" Hamiltonian composed of two parts, ch (the chromophore which is directly coupled to the applied field) and b (the bath) weakly coupled by $\hat{V}$, we arrive at an equation of motion for the reduced chromophore density matrix σ through application of standard Redfield theory[48,49]

$$\dot{\sigma}_{ij}(t) = -i\omega_{ij}\sigma_{ij} + \mathbb{L}^{E}_{ij;kl}(t)\sigma_{kl} + \mathbb{L}^{\Gamma}_{ij;kl}\sigma_{kl} + \mathbb{R}_{ij;kl}\sigma_{kl} \equiv \mathbb{L}_{ij;kl}(t)\sigma_{kl} \tag{7}$$

Here, the matrix $\mathbb{R}$ is the usual Redfield matrix to account for bath perturbations on the chromophore and the matrix $\mathbb{L}(t)$ reflects the entire dynamics for σ. We note that additivity of contributions stemming from quantum field, bath, and classical (laser) field perturbations to the dynamics of the chromophore should be viewed as an approximation of "independent rates of variation".[46] We neglect frequency shifts of the chromophore due to $\hat{V}$, so that the labels ij now correspond to the eigenstates of H^{ch}. We consider this set of approximations as the natural extension of the optical Bloch equations to multi-level systems in a condensed phase. Specification of the matrices $\mathbb{L}^{E}$, $\mathbb{L}^{\Gamma}$, and $\mathbb{R}$ will allow us to apply this formalism to various physical problems, and several model systems will be considered in the following sections.

B. Extraction of Photon Counting Moments. Extending the picture of the preceding section to calculation of photon counting statistics for single molecule measurements proceeds in a manner analogous to the case for two-level chromophores.[37,40] The formal solution has been presented in ref 41, and we present here a brief derivation following ref 37 to clarify our notation and to extend this picture to the calculation of photon counting moments for individual spontaneous emission transitions (as will be useful in spectrally resolved emission spectroscopy).

Imagine a detector capable of differentiating between photons that are emitted for particular chromophore transitions. In certain cases, this would be possible by only selecting photons within a certain frequency window, in other cases this might not be experimentally feasible but should be regarded as a gedanken experiment. That portion of $\mathbb{L}(t)$ responsible for placing the chromophore in a lower energy state immediately following the transition of interest is of special importance for calculating statistics associated with this transition. From eq 4, this is the element $\mathbb{L}^{+\Gamma}_{bb;aa}$ with the numerical value Γ_{ab}, assuming that we are following $a \rightarrow b$ emissions. We partition eq 7 to give this single part of the evolution a unique status

$$\dot{\sigma}_{ij}(t) = \mathbb{L}'_{ij;kl}(t)\sigma_{kl} + \Gamma_{ab}\delta_{ij,bb}\delta_{kl;aa}\sigma_{kl} \equiv \mathbb{L}'_{ij;kl}(t)\sigma_{kl} + \mathbb{L}^{+\Gamma_{ab}}_{ij;kl}\sigma_{kl} \tag{8}$$

where $\mathbb{L}'(t)$ is that portion of $\mathbb{L}(t)$ not pulled out in $\mathbb{L}^{+\Gamma_{ab}}$. In exact analogy to the case with only a two-level chromophore, it is the operator $\mathbb{L}^{+\Gamma_{ab}}$ that dictates when an $a \rightarrow b$ spontaneous emission event occurs. Following exactly the same arguments as in ref 37 allows us to write

$$\dot{\sigma}^{(n)}_{ij}(t) = \mathbb{L}'_{ij;kl}(t)\sigma^{(n)}_{kl} + \mathbb{L}^{+\Gamma_{ab}}_{ij;kl}\sigma^{(n-1)}_{kl} \tag{9}$$

where $\sigma^{(n)}$ is that portion of the reduced density matrix corresponding to systems that have previously emitted exactly n photons via $a \rightarrow b$ transitions.

To facilitate the extraction of photon counting moments, we introduce a generating function version of eq 9

$$\dot{\mathscr{G}}_{ij}(t,s) = \mathbb{L}'_{ij;kl}(t)\mathscr{G}_{kl}(t,s) + s\mathbb{L}^{+\Gamma_{ab}}_{ij;kl}\mathscr{G}_{kl}(t,s) = \mathbb{L}_{ij;kl}(t,s)\mathscr{G}_{kl}(t,s)$$

$$\mathscr{G}(t,s) \equiv \sum_{n=0}^{\infty} s^n \sigma^{(n)}(t) \tag{10}$$

The actual generating function for $a \rightarrow b$ photon emissions is obtained by summing over all "population" elements of $\mathscr{G}(s,t)$

$$G(s,t) = \sum_i \mathscr{G}_{ii}(s,t) \tag{11}$$

which allows for the usual extraction of probabilities for n photon emissions[50]

$$p_n(t) = \frac{1}{n!}\frac{\partial^n}{\partial s^n} G(s,t)\Big|_{s=0} \tag{12}$$

and factorial moments[50]

$$\langle n^{(m)}\rangle(t) \equiv \langle n(n-1)(n-2)\ldots(n-m+1)\rangle(t) = \frac{\partial^m}{\partial s^m} G(s,t)\Big|_{s=1} \tag{13}$$

Our primary concern in this work shall be the calculation of moments. To this end, we differentiate eq 10 with respect to s yielding equations for the $\partial^m/\partial s^m \mathscr{G}$ elements which, when summed over population elements, yield the moments (when $s = 1$).

$$\frac{\partial}{\partial t}\left(\frac{\partial^m \mathscr{G}(s,t)}{\partial s^m}\right) = \mathbb{L}(t,s)\left(\frac{\partial^m \mathscr{G}}{\partial s^m}\right) + m\mathbb{L}^{+\Gamma_{ab}}\left(\frac{\partial^{m-1}\mathscr{G}}{\partial s^{m-1}}\right) \tag{14}$$

The high-order derivatives are dependent upon all lower derivatives as can be seen by iterating this equation. For example, moments up to and including second order are generated by solving the set of equations

$$\begin{pmatrix} \dot{\mathscr{G}}(s,t) \\ \dfrac{\partial \dot{\mathscr{G}}(s,t)}{\partial s} \\ \dfrac{\partial^2 \dot{\mathscr{G}}(s,t)}{\partial s^2} \end{pmatrix} = \begin{pmatrix} \mathbb{L}(t,s) & 0 & 0 \\ \mathbb{L}^{+\Gamma_{ab}} & \mathbb{L}(t,s) & 0 \\ 0 & 2\mathbb{L}^{+\Gamma_{ab}} & \mathbb{L}(t,s) \end{pmatrix} \cdot \begin{pmatrix} \mathscr{G}(s,t) \\ \dfrac{\partial \mathscr{G}(s,t)}{\partial s} \\ \dfrac{\partial^2 \mathscr{G}(s,t)}{\partial s^2} \end{pmatrix} \tag{15}$$

Evaluation at $s = 1$ provides the moments up to second order by way of eq 13. Since $\mathbb{L}(t,s)$ and $\mathbb{L}^{+\Gamma_{ab}}$ are $N^2 \times N^2$ matrices for a quantum system with N states, the above expression

corresponds to solving $3N^2$ coupled equations. In the cases considered in this work, we will take $\boldsymbol{E}(t)$ to have sinusoidal time dependence so that the explicit time dependence within $\mathbb{L}(t)$ may be removed by moving to a rotating reference frame and applying the rotating wave approximation (RWA). In this case, solution of these equations is easily accomplished by directly exponentiating the $3N^2 \times 3N^2$ matrix as outlined in the next section. Equation 15 is central to all results in this paper and, in principle, could have been directly solved to reproduce all the calculations presented below. In practice, we used a numerically simpler scheme to obtain our results derived from eq 15. This numerical technique is elaborated on in section IID. Formation of the matrices $\mathbb{L}(t,s)$ and $\mathbb{L}^{+\Gamma_{ab}}$ for use in any numerical scheme follow from the preceding section. Specific choices for these matrixes depend on the physical systems under consideration and will be detailed with presentation of our chosen applications.

The above derivation has assumed that we are interested in the statistics of photons emitted from one particular chromophore transition ($a \rightarrow b$). When we are interested in broadband detection with all photons counted equivalently, the structure of eq 15 remains unchanged. However, the matrices $\mathbb{L}(t,s)$ and $\mathbb{L}^{+\Gamma_{ab}}$ have different forms. In that case, we substitute $\mathbb{L}^{+\Gamma}$ for $\mathbb{L}^{+\Gamma_{ab}}$ and $\mathbb{L}(t,s)$ is now the matrix formed by appending s to every spontaneous emission matrix element within $\mathbb{L}(t)$ having a positive sign (i.e., the whole of $\mathbb{L}^{+\Gamma}$). Calculation of moments for photons associated with some subset of transitions (perhaps transitions inside a certain frequency window) proceeds by generalizing to placement of s variables only on the elements associated with the relevant transitions and making the corresponding changes to $\mathbb{L}^{+\Gamma}$. In principle, we could introduce a number of different auxiliary variables—each variable corresponding to a particular transition or subset of transitions. This leads to expressions for cross correlations between various transitions. The extension is straightforward, but not explicitly presented here, as we do not calculate any such cross correlations in this work.

C. Model Hamiltonians and Practical Considerations. In this work, we shall be concerned exclusively with model systems consisting of a chromophore with two electronic states (ground $|g\rangle$ and excited $|e\rangle$), so that

$$\hat{H}^{\mathrm{ch}} = |g\rangle H_{\mathrm{g}} \langle g| + |e\rangle H_{\mathrm{e}} \langle e| \tag{16}$$

H_{g} and H_{e} are, respectively, the chromophore Hamiltonians for nuclear motion within the ground and excited states, with eigenfunctions and eigenvalues specified by

$$H_{\mathrm{g}}|n_g\rangle = \epsilon_{n_g}|n_g\rangle$$

$$H_{\mathrm{e}}|m_e\rangle = \epsilon_{m_e}|m_e\rangle \tag{17}$$

for $m_e = 1...N_e$, $n_g = 1,...N_g$. In our numerical applications, we consider only a finite number of eigenstates associated with nuclear motion and adopt the convention here. The nuclear ground state in the excited manifold is assumed to lie higher in energy than the nuclear ground state of the ground manifold by an amount $\hbar\omega_{eg}$. It is to be understood that this chromophore Hamiltonian dictates dynamics in the sense implied by eq 6. $\hat{H}^{\mathrm{ch}}$ is responsible for the evolution that we designate to be the most important to chromophore dynamics. The effect of the environment (bath) will be felt through coupling dictated by $\hat{V}$.

Interactions with the radiation field depend on the matrix elements of the system's dipole moment operator as evidenced by eq 2 and the presence of $\hat{\boldsymbol{\mu}}$ in $\mathbb{L}^E(t)$. We treat these matrix elements in the Condon approximation[47] such that

$$\boldsymbol{D}_{n_g;m_e} = \langle g|\hat{\boldsymbol{\mu}}|e\rangle\langle n_g|m_e\rangle \equiv \boldsymbol{\mu}_0\langle n_g|m_e\rangle \tag{18}$$

The dipole operator is assumed to act solely in the electronic space with only off-diagonal coupling between ground and excited states. Individual transition intensities are mediated by the overlap of nuclear wave functions. We always consider a monochromatic exciting field of constant intensity and polarization direction, so that

$$\mathbf{E}(t) = \boldsymbol{\epsilon}_0 \cos(\omega_L t) \tag{19}$$

For future notational simplicity, we define constants Γ_0 and Ω_0 as

$$\Gamma_0 = \frac{\omega_{eg}{}^3|\boldsymbol{\mu}_0|^2}{3\pi\epsilon\hbar c^3}$$

$$\Omega_0 = \boldsymbol{\epsilon}_0 \cdot \boldsymbol{\mu}_0/\hbar \tag{20}$$

These constants represent the spontaneous emission rate and Rabi frequency for an electronic transition between states with perfect overlap of nuclear wave functions.

These definitions allow us to specify the form of matrices $\mathbb{L}^E(t)$ and $\mathbb{L}^\Gamma$. $\mathbb{L}^\Gamma$ follows immediately from eq 4. All we need are the emission rates Γ_{ij} for all $i \rightarrow j$ transitions. Since our models only allow transitions between excited and ground electronic states, we need only consider rates of the form $\Gamma_{|e\rangle|m_e\rangle;|g\rangle|n_g\rangle} \equiv \Gamma_{m_e n_g}$ with values

$$\Gamma_{m_e n_g} = \Gamma_0 |\langle m_e|n_g\rangle|^2 \tag{21}$$

All positions in the $\mathbb{L}^\Gamma$ diagonal in the electronic subspace are necessarily zero due to our assumptions about the dipole operator, so the above completely specifies the $\mathbb{L}^\Gamma$ matrix.

The formation of $\mathbb{L}^E(t)$ is slightly more complicated due to the nature of the coupling to the applied field, which makes for a matrix less sparse than the emission matrix. We first realize that, as in the usual optical Bloch equations, density matrix elements diagonal in the electronic subspace are coupled to those off-diagonal in the electronic subspace and vice versa. Also, by analogy to the optical Bloch equations we retain only those terms corresponding to resonant excitation by the field (i.e., a photon is absorbed and electronic state rises or a photon is emitted and state drops) by invoking the Rotating wave approximation (RWA).[46] We make use of the definition

$$\Omega_{m_e n_g} = \Omega_0 |\langle m_e|n_g\rangle| \tag{22}$$

to give the elements of $\mathbb{L}\boldsymbol{E}(t)$ within the RWA

$$\mathbb{L}^E_{n_g m_g;k_e l_g} = -\overline{\mathbb{L}^E_{k_e l_g;n_g m_g}} = +\frac{i}{2}\Omega_{n_g k_e} e^{i\omega_L t}\delta_{m_g,l_g} \tag{23}$$

$$\mathbb{L}^E_{n_g m_g;k_g l_e} = -\overline{\mathbb{L}^E_{k_g l_e;n_g m_g}} = -\frac{i}{2}\Omega_{l_e m_g} e^{-i\omega_L t}\delta_{n_g,k_g}$$

$$\mathbb{L}^E_{n_e m_e;k_e l_g} = -\overline{\mathbb{L}^E_{k_e l_g;n_e m_e}} = -\frac{i}{2}\Omega_{l_g m_e} e^{i\omega_L t}\delta_{n_e,k_e}$$

$$\mathbb{L}^{E}_{n_e m_e;k_g l_e} = -\overline{\mathbb{L}^{E}_{k_g l_e;n_e m_e}} = +\frac{i}{2}\Omega_{n_e k_g} e^{-i\omega_L t}\delta_{m_e,l_e} \quad (24)$$

Overbars represent complex conjugation. (The above definitions assume that our dipole operator matrix elements are real quantities.)

The only portion of $\mathbb{L}(t)$ remaining to be specified is the Redfield matrix for transitions of the chromophore induced by environmental bath fluctuations, $\mathbb{R}$. The relaxation matrix is given by[48,49]

$$\mathbb{R}_{ij;kl} = -\delta_{ik}\sum_r t^-_{lrrj} - \delta_{lj}\sum_r t^+_{irrk} + t^-_{jlik} + t^+_{jlik} \quad (25)$$

where

$$t^+_{ljik} = \frac{1}{\hbar^2}\int_0^\infty d\tau e^{-i\omega_{ik}\tau}\langle \hat{V}_{lj}(\tau)\hat{V}_{ik}(0)\rangle_b$$

$$t^-_{ljik} = \frac{1}{\hbar^2}\int_0^\infty d\tau e^{-i\omega_{ij}\tau}\langle \hat{V}_{lj}(0)\hat{V}_{ik}(\tau)\rangle_b \quad (26)$$

are Fourier−Laplace transforms of the correlation functions of the system and bath coupling at the specified frequency. The bath-space Heisenberg operators are defined by

$$\hat{V}_{ki}(\tau) = e^{i/\hbar\hat{H}^b\tau}\hat{V}_{ki}e^{-i/\hbar\hat{H}^b\tau}$$

$$\hat{V}_{ki} = \langle k|\hat{V}|i\rangle \quad (27)$$

and the averages $\langle ...\rangle_b$ specify a thermal average over bath degrees of freedom only. In all models we consider, bath fluctuations are capable of causing transitions between levels within a particular electronic state but are not permitted to induce radiationless transitions between electronic states. Further discussion on the evaluation of $\mathbb{R}$ will appear in sections III and IV as specific models for chromophore and bath are introduced.

Given the particular form of our model systems, it is highly beneficial to solve eq 7 in a rotating reference frame by introducing new variables

$$\tilde{\sigma}_{n_g m_e} = \sigma_{n_g m_e}e^{-i\omega_L t}$$

$$\tilde{\sigma}_{n_e m_g} = \sigma_{n_e m_g}e^{i\omega_L t}$$

$$\tilde{\sigma}_{n_e m_e} = \sigma_{n_e m_e}$$

$$\tilde{\sigma}_{n_g m_g} = \sigma_{n_g m_g} \quad (28)$$

The primary advantage of this formulation being that eq 7 is recast in a form without explicit time dependence

$$\dot{\tilde{\sigma}}_{ij}(t) = -i\mathbb{W}_{ij,kl}\tilde{\sigma}_{kl} + \mathbb{L}^{E}_{ij;kl}\tilde{\sigma}_{kl} + \mathbb{L}^{\Gamma}_{ij;kl}\tilde{\sigma}_{kl} + \mathbb{R}_{ij;kl}\tilde{\sigma}_{kl} \equiv \mathbb{L}_{ij;kl}\tilde{\sigma}_{kl} \quad (29)$$

where the diagonal matrix $\mathbb{W}$ is given by

$$\mathbb{W}_{n_g m_g;n_g m_g} = \omega_{n_g m_g}$$

$$\mathbb{W}_{n_e m_e;n_e m_e} = \omega_{n_e m_e}$$

$$\mathbb{W}_{n_e m_g;n_e m_g} = \omega_{n_e m_g} - \omega_L$$

$$\mathbb{W}_{n_g m_e;n_g m_e} = \omega_{n_g m_e} + \omega_L \quad (30)$$

The matrix $\mathbb{L}^E$ is simply the matrix specified by eq 23, evaluated at $t = 0$, and the remaining matrices are unchanged relative to the original basis. Since the populations of $\tilde{\sigma}$ are identical to σ, we may calculate photon emission statistics using these transformed variables without any changes to the formalism of the preceding subsection. In particular, we may calculate eq 15 as

$$\begin{pmatrix} \dot{\tilde{\mathcal{G}}}(s,t) \\ \dfrac{\partial\dot{\tilde{\mathcal{G}}}(s,t)}{\partial s} \\ \dfrac{\partial^2\dot{\tilde{\mathcal{G}}}(s,t)}{\partial s^2} \end{pmatrix} = \begin{pmatrix} \mathbb{L}(s) & 0 & 0 \\ \mathbb{L}^{+\Gamma_{ab}} & \mathbb{L}(s) & 0 \\ 0 & 2\mathbb{L}^{+\Gamma_{ab}} & \mathbb{L}(s) \end{pmatrix} \cdot \begin{pmatrix} \tilde{\mathcal{G}}(s,t) \\ \dfrac{\partial\tilde{\mathcal{G}}(s,t)}{\partial s} \\ \dfrac{\partial^2\tilde{\mathcal{G}}(s,t)}{\partial s^2} \end{pmatrix} \quad (31)$$

where the time-independent $\mathbb{L}$ is specified by eq 29 and $\tilde{\mathcal{G}}(s,t)$ is given by

$$\tilde{\mathcal{G}}(t,s) \equiv \sum_{n=0}^{\infty} s^n\tilde{\sigma}^{(n)}(t) \quad (32)$$

Summing over the "population" elements of $\tilde{\mathcal{G}}$ still returns the original generating function for photon emissions, $G(s,t)$, so calculations in this frame return emission statistics equivalent to the original formulation. Numerics in this basis are preferred, since eq 31 may be solved simply by direct matrix exponentiation.

D. Reported Quantities and Numerical Details. The bulk of the preceding sections has been devoted to establishing models for reduced chromophore dynamics, that is, how to specify the superoperator matrix $\mathbb{L}(t)$ in eq 7 or the corresponding time-independent matrix $\mathbb{L}$ in eq 29. Given this matrix, it is a trivial programming task to extend the standard calculation of density matrix evolution to photon counting observables. The matrix $\mathbb{L}(s)$ is formed by appending the auxiliary variable s to elements of $\mathbb{L}^{+\Gamma}$ reflecting spontaneous emission transitions of interest. In the case of a single relevant transition, only one element is modified. In broadband detection, we append an s to the entire $\mathbb{L}^{+\Gamma}$ matrix. Given $\mathbb{L}(s)$, the block form of eq 31 follows immediately and calculation of $\tilde{\mathcal{G}}$ is provided by simple matrix exponentiation. Summing over population elements of $\partial^m\tilde{\mathcal{G}}(s,t)/\partial s^m$ for $s = 1$ yields the factorial photon counting moment of order m. Although the matrix in eq 31 is specific to calculation of $m = 2$, higher order moments can be calculated in analogous fashion by extending the block matrix as implied by eq 15. Since we assume no photon emissions prior to $t = 0$, the initial condition employed in eq 31 is simply $\tilde{\mathcal{G}}_{ij}(s,0) = \tilde{\sigma}_{ij}(0)$ with all s derivatives of $\tilde{\mathcal{G}}$ equal to zero.

The moments reported in this work will be presented in terms of absorption and emission line shapes and corresponding Mandel Q parameter[51] spectra. Mandel's Q parameter is related to the factorial moments via

$$Q(t) \equiv \frac{\langle n^2\rangle(t) - \langle n\rangle^2(t)}{\langle n\rangle(t)} - 1 \quad (33)$$

and serves as a convenient means to report second-order photon statistics. Positive Q values reflect photon bunching behavior (an elevated variance in n relative to Poisson processes with the same mean), negative Q values reflect antibunching behavior (diminished variance in n relative to a Poisson process with the same mean), and $Q = 0$ is consistent with purely Poissonian statistics.

Energy conservation implies that we may calculate absorption line shapes, by counting the relative rate of photon emission (photons from all transitions are counted) as a function of the exciting frequency

$$I(\omega_L) = \lim_{t\to\infty} \frac{\partial}{\partial t}\langle n\rangle(t) \equiv \lim_{t\to\infty} \frac{\partial}{\partial t}\left[\frac{\partial}{\partial s} G(s,t)\Big|_{s=1}\right] \qquad (34)$$

Every emitted photon corresponds to a prior excitation of the chromophore and hence a quantum of energy ($\hbar\omega_L$) extracted from the incident field. We evaluate line shapes in the limit of long times to ensure that the system is in a steady state. The time dependence of $d\langle n\rangle/dt$ at early times is interesting as well[36,37] but not specifically considered in this work. The Q parameter absorption spectra are calculated in analogous fashion, although the definition of Q, with $\langle n\rangle(t)$ in the denominator, ensures saturation to a constant value as time becomes large; the Q parameter itself as a function of exciting frequency is reported. Again, in the "absorption Q spectra", we collect all photon emissions (broadband detection).

Emission line shapes and the Q parameter are calculated in similar fashion, but we resolve the photon statistics by frequency of the emitted photons. More precisely, we resolve by the transitions where the photons originate from.

In the cases we consider, the allowed transitions are either well resolved in frequency (frequency differences much larger than natural line widths) or perfectly degenerate, so that there is no ambiguity in assigning photons to a particular frequency "window". We report our results as

$$I(\omega_E;\omega_L) = \lim_{t\to\infty} \frac{\partial}{\partial t}\langle n_{\omega_{ij}=\omega_E}\rangle(t) \qquad (35)$$

The above notation specifies that we only consider photons from transitions on resonance with ω_E. A collection of these statistics follows the prescription previously described. The matrix $\mathbb{L}(s)$ depends on ω_E as placement of s variables is dictated by which transitions are on resonance with ω_E. We note that our emission "spectra" are thus not quite spectra in the usual sense. Our spectral lines are infinitely sharp, without broadening (see Figure 5). In principle, we could artificially broaden these lines by making them Lorentzians with the natural line width of each transition, but we have not done so. What our calculations directly provide are the statistics associated with particular molecular transitions, not the actual frequency of the emitted photons. Note that our line shapes will also, in general, depend on the frequency of the exciting light as different excitations can lead to different steady-state populations of the chromophore.

The Q parameter emission spectrum follows similarly

$$Q(\omega_E;\omega_L) \equiv \frac{\langle n^2{}_{\omega_{ij}=\omega_E}\rangle - \langle n_{\omega_{ij}=\omega_E}\rangle^2}{\langle n_{\omega_{ij}=\omega_E}\rangle} - 1 \qquad (36)$$

where we stress that the photon numbers n collected above reflect only those photons stemming from transitions on resonance with ω_E.

For multi-level quantum systems, the matrix of eq 31 can become very large ($3N^2 \times 3N^2$ for N quantum levels). If moments higher than second order are desired, then the matrix becomes even bigger. Direct exponentiation of such matrices over a wide range of frequencies is computationally expensive and, for sufficiently large N and/or moment order, eventually becomes computationally intractable. In this work, we focus on statistics calculated in the long time (steady state) limit. For direct exponentiation, this limit has the additional computational complications associated with the identification of a time sufficiently large for the steady state to be attained, yet sufficiently small to ensure numerical stability. When only steady-state information is desired, analytical progress can be made on eq 31, allowing calculation to proceed via diagonalization of matrixes no larger than $N^2 \times N^2$ and without the need to identify a suitable finite time at which the long time limit is reached. The calculation is summarized below.

The equations of motion for $\tilde{\mathscr{G}}$ and its s derivatives (eq 31) can be formally integrated to yield

$$\tilde{\mathscr{G}}'(t) = \int_0^t dt' e^{\mathbb{L}(t-t')}\,\mathbb{L}^{+\Gamma}\rho_{ss}$$

$$\tilde{\mathscr{G}}''(t) = 2\int_0^t dt' e^{\mathbb{L}(t-t')}\,\mathbb{L}^{+\Gamma}\int_0^{t'} dt'' e^{\mathbb{L}(t'-t'')}\,\mathbb{L}^{+\Gamma}\rho_{ss} \qquad (37)$$

Here, we have assumed that the system began in the steady state at $t = 0$ and that we began counting photons at $t = 0$ (different initial conditions lead to negligible corrections in the long time limit). We have introduced a prime notation for s derivatives (i.e., $(\partial\tilde{\mathscr{G}}/\partial s) \equiv \tilde{\mathscr{G}}'$) and we have evaluated everything for $s = 1$. The steady-state limit for the density matrix ρ_{ss} is expected on physical grounds for systems driven by external perturbations and allowed to relax via radiative and nonradiative transitions—its existence was verified for the model systems studied in this work.

The matrix $\mathbb{L}$ may be diagonalized, and we write $\Lambda = \chi^{-1}\mathbb{L}\chi$ with Λ the diagonal representation of $\mathbb{L}$. The columns of χ consist of the right eigenvectors of $\mathbb{L}$, and the rows of χ^{-1} are the left eigenvectors of $\mathbb{L}$. The associated eigenvalues of $\mathbb{L}$ are complex numbers with negative real parts, except the single eigenvalue associated with the steady state which is zero. Ordering the eigenvalues $\{\lambda_{ss} = 0, \lambda_2, \lambda_3, ...\}$, so that

$$\Lambda = \begin{pmatrix} 0 & 0 & 0 & \cdots \\ 0 & \lambda_2 & 0 & \cdots \\ 0 & 0 & \lambda_3 & \cdots \\ \vdots & \vdots & \vdots & \ddots \end{pmatrix} \qquad (38)$$

we see that it is possible to partition the time evolution operator $U(\tau) = e^{\mathbb{L}\tau} \equiv U_0 + U_1(\tau)$ into two pieces such that the first corresponds to the (lack of) evolution of the steady state and the second piece reflects all other dynamics in the system.

$$U_0 = \chi\begin{pmatrix} 1 & 0 & 0 & \cdots \\ 0 & 0 & 0 & \cdots \\ 0 & 0 & 0 & \cdots \\ \vdots & \vdots & \vdots & \ddots \end{pmatrix}\chi^{-1}$$

$$U_1(\tau) = \chi\begin{pmatrix} 0 & 0 & 0 & \cdots \\ 0 & e^{\lambda_2\tau} & 0 & \cdots \\ 0 & 0 & e^{\lambda_3\tau} & \cdots \\ \vdots & \vdots & \vdots & \ddots \end{pmatrix}\chi^{-1}$$

Partitioning the matrices in this way allows us to explicitly carry out the integrations in eq 37 to give (large time limit assumed)

$$\tilde{\mathscr{G}}' = (tU_0 + X)\,\mathbb{L}^{+\Gamma}\rho_{ss}$$

$$\tilde{\mathscr{G}}'' = t^2(U_0\mathbb{L}^{+\Gamma})^2\rho_{ss} + 2t(U_0\mathbb{L}^{+\Gamma}X\mathbb{L}^{+\Gamma} + X\mathbb{L}^{+\Gamma}U_0\mathbb{L}^{+\Gamma})\rho_{ss}$$

$$X \equiv \chi \begin{pmatrix} 0 & 0 & 0 & \cdots \\ 0 & -\lambda_2^{-1} & 0 & \cdots \\ 0 & 0 & -\lambda_3^{-1} & \cdots \\ \vdots & \vdots & \vdots & \ddots \end{pmatrix} \chi^{-1} \tag{39}$$

The long time (steady state) limit for the rate of photon emission (intensity) and the Q parameter follow immediately

$$\frac{d\langle n\rangle}{dt} = \sum_{PE} U_0\mathbb{L}^{+\Gamma}\rho_{ss}$$

$$Q = 2\,\frac{\sum_{PE} U_0\mathbb{L}^{+\Gamma}X\mathbb{L}^{+\Gamma}\rho_{ss}}{\sum_{PE} U_0\mathbb{L}^{+\Gamma}\rho_{ss}} \tag{40}$$

where the summations are over the population elements of the resulting vectors.

Equation 40 was used in the computation of all quantities reported in the examples discussed below. We stress that no approximations have been introduced into these equations. The simplifications we obtain are due to the fact that we only consider the infinite time limit in eq 40. The numerical advantages of eq 40 relative to direct matrix exponentiation are manyfold. First, it is not necessary to pick a time to evaluate your expressions and somehow confirm that this time is both large enough to ensure the steady state yet small enough to avoid numerical instabilities. Equation 40 assumes $t \rightarrow \infty$. Using this method one only has to find the eigenvalues and eigenvectors of the matrix $\mathbb{L}$ for a given excitation frequency to obtain both the intensity and the Q parameter. This matrix is 3 times smaller in the linear dimension than the matrix that must be exponentiated to solve eq 31. If higher moments are required, one still has only to diagonalize the $\mathbb{L}$ matrix for use in expressions similar to eq 39. Finally, while matrix exponentiation requires that one repeat the entire calculation to obtain statistics for various detection possibilities (broadband, a single transition counted, several transitions counted, etc.), the present scheme only requires a single diagonalization for all possible detection schemes. Different detection possibilities manifest themselves only through the matrix $\mathbb{L}^{+\Gamma}$ which does not have to be diagonalized. The pieces of eq 40 dependent on matrix diagonalization (X, U_0, ρ_{ss}) do not vary with different detection schemes. This is a significant computational advantage when calculating emission spectra since the bulk of the calculation need only be performed a single time.

III. Chromophore Coupled to a Two-Level System

A. Model Description. As a first example, we consider the case of a chromophore coupled to a two-level system (TLS). The two-level system model is of interest both for theoretical reasons (it is arguably the simplest case of dynamics beyond that of an isolated two-level chromophore) and also for its utility in describing the thermal behavior of low-temperature glasses.[52,53] The model is also frequently applied to the spectroscopy of chromophores embedded in low-temperature glasses.[54] Although TLS dynamics is often treated as a purely stochastic perturbation of the chromophore system, we adopt a more precise, quantum mechanical picture here. The following description of coupled chromophore−TLS dynamics is quite terse. We refer readers to the review by Silbey[54] for more detail on the Redfield dynamics that we employ.

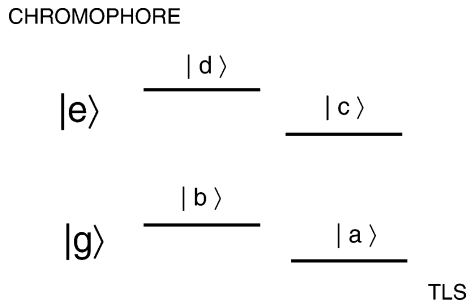

Figure 1. Energy level diagram for the composite chromophore−TLS system.

The nature of TLS dynamics within the glass is presumably the localized rearrangement of a small cluster of atoms[52,53] corresponding to movement between two distinct energy minima. The coupling between TLS and chromophore enters as a different effective splitting between chromophore ground and excited states depending on which minima the TLS resides in. Assuming this coupling is due to strain dipole interactions between chromophore and TLS, we expect the interaction to scale as $1/r^3$ in the distance between TLS and chromophore centers.[54] The basis of TLS "minima" states is not expected to be diagonal as tunneling may occur between minima. In addition, coupling between the TLS and long wavelength phonons in the glass acts as mechanism for coupling the TLS−chromophore system to its glassy environment. Adopting the notation of section IIC, the mathematical formulation of this picture is[54,55]

$$H_g = -\frac{\hbar\omega_{eg}}{2} + \left(\frac{A}{2} - \frac{\alpha}{4r^3}\right)\sigma_z^{TLS} + \frac{J}{2}\sigma_x^{TLS}$$

$$H_e = +\frac{\hbar\omega_{eg}}{2} + \left(\frac{A}{2} + \frac{\alpha}{4r^3}\right)\sigma_z^{TLS} + \frac{J}{2}\sigma_x^{TLS}$$

$$\hat{V} = \sum_q g_q(b_{-q}^\dagger + b_q)\,\sigma_z^{TLS}$$

$$\hat{H}^b = \sum_q b_q^\dagger b_q \hbar\omega_q \tag{41}$$

Here, A and J are, respectively, the asymmetry and tunneling matrix element for the TLS and σ_z^{TLS} and σ_x^{TLS} are Pauli matrices in the basis of TLS localized "minima" states. ω_{eg} is the chromophore transition frequency in the absence of interactions. The index q labels the phonon modes of the system, and $b_q^\dagger$, b_q, ω_q, and g_q are the creation operator, annihilation operator, frequency, and TLS strain field coupling constants for the qth mode.

We diagonalize the chromophore−TLS portion of our Hamiltonian and label the four eigenstates $|a\rangle$, $|b\rangle$, $|c\rangle$, and $|d\rangle$ (see Figure 1) in order of increasing energy (we assume $\hbar\omega_{eg}$ to be by far the largest energy scale in the problem). In this basis, eq 41 can be written

$$H_g = \omega_a|a\rangle\langle a| + \omega_b|b\rangle\langle b|$$

$$H_e = \omega_c|c\rangle\langle c| + \omega_d|d\rangle\langle d|$$

$$\hat{V} = \sum_q g_q(b_{-q}^\dagger + b_q)\left[\frac{J}{\omega_g}(|b\rangle\langle a| + |a\rangle\langle b|) + \frac{J}{\omega_e}(|c\rangle\langle d| + |d\rangle\langle c|)\right] \quad (42)$$

where ω_a, ω_b, ω_c, ω_d, ω_g, and ω_e are the frequencies

$$\omega_a = -\frac{1}{2}\omega_{eg} - \frac{1}{2}\sqrt{J^2 + (A-P)^2}$$

$$\omega_b = -\frac{1}{2}\omega_{eg} + \frac{1}{2}\sqrt{J^2 + (A-P)^2}$$

$$\omega_c = +\frac{1}{2}\omega_{eg} - \frac{1}{2}\sqrt{J^2 + (A+P)^2}$$

$$\omega_d = +\frac{1}{2}\omega_{eg} + \frac{1}{2}\sqrt{J^2 + (A+P)^2}$$

$$\omega_g = \omega_b - \omega_a$$

$$\omega_e = \omega_d - \omega_c \quad (43)$$

and we have set $(P/2) \equiv (\alpha/4r^3)$. Note that we have intentionally omitted all (system) diagonal contributions to the system−bath coupling since these terms will yield no contribution to the Redfield matrix.

Specification of $\mathbb{R}$ is quite simple (if tedious) and proceeds by calculating the terms specified in eqs 25 and 26. Since the bath is formed by a set of bosons (phonons), evaluation of the correlation functions is dictated by the well-known properties of these operators. In particular since

$$b_q(t) = e^{-i\omega_q t}b_q(0)$$

$$b_q^\dagger(t) = e^{+i\omega_q t}b_q^\dagger(0)$$

$$\langle b_q b_q^\dagger\rangle_b = (1 - e^{-\beta\hbar\omega_q})^{-1}$$

$$\langle b_q^\dagger b_q\rangle_b = e^{-\beta\hbar\omega_q}(1 - e^{-\beta\hbar\omega_q})^{-1} \quad (44)$$

the correlation functions become

$$\langle \hat{V}_{ij}(\tau)\hat{V}_{kl}(0)\rangle_b = \sum_q g_q^{ij} g_q^{kl}(1 - e^{-\beta\hbar\omega_q})^{-1}[e^{-i\omega_q\tau} + e^{-\beta\hbar\omega_q}e^{i\omega_q\tau}] \quad (45)$$

The coupling constants g_q are chosen to reflect strain field coupling between TLS and the phonon bath;[54] they scale with q as $q^{1/2}$. The ij and kl suffixes on g_q indicate that there are additional constants that need to be included—either J/ω_e or J/ω_g depending on which specific terms the indices refer to. Integration in time over these terms as specified by eq 26 serves to create a delta function in frequency which makes evaluation of the sum over q trivially easy if we approximate the sum as an integral. By this approach, we calculate, for example

$$\mathbb{R}_{cc;dd} = e^{\beta\hbar\omega_e}\mathbb{R}_{dd;cc} = C\omega_e J^2 \frac{1}{1 - e^{-\beta\hbar\omega_e}}$$

$$\mathbb{R}_{aa;bb} = e^{\beta\hbar\omega_g}\mathbb{R}_{bb;aa} = C\omega_g J^2 \frac{1}{1 - e^{-\beta\hbar\omega_g}}$$

$$\mathbb{R}_{ca;db} = \frac{1}{2}\left[\frac{\omega_e}{\omega_g}\mathbb{R}_{cc;dd} + \frac{\omega_g}{\omega_e}\mathbb{R}_{aa;bb}\right]$$

$$\mathbb{R}_{db;ca} = \frac{1}{2}\left[\frac{\omega_e}{\omega_g}\mathbb{R}_{dd;cc} + \frac{\omega_g}{\omega_e}\mathbb{R}_{bb;aa}\right] \quad (46)$$

where C is a collection of constants incorporating the coupling strength between TLS and bath, which is typically taken as a parameter used to fit experiment rather than estimated from first principles.[14] Of course, the top two lines just express the phonon assisted transition rates from state d to c and b to a as expected. Other elements follow similarly. We make no effort to implement the customary secular approximations to these equations as the equations are solved numerically and the highly oscillatory terms will remove themselves from consideration naturally.

B. Numerical Results. In this section, we present numerical results for the model system described above. The framework for calculating the fully quantum dynamical results are spelled out in section II. Physical constants have been chosen to correspond with typical situations for a glassy material.[14,55] To compare with our previous work on stochastic models, it is necessary to map the above quantum description to a stochastic picture. Details for calculating photon statistics for a stochastic TLS coupled to a chromophore have been presented in detail elsewhere.[37] Readers are referred there for a discussion, where we have employed notation identical to the present work. Determination of appropriate model parameters for the stochastic model, based upon the above quantum picture, is well established.[54] In the stochastic picture, the TLS acts solely to modulate the transition frequency of the chromophore, causing hops between $\omega_{eg} + \nu$ and $\omega_{eg} - \nu$. The rate of hopping is given by $R_\uparrow$ for transitions to the less thermally occupied TLS state and $R_\downarrow$ for the reverse direction. The difference in energy of the two TLS states is provided by detailed balance. Correspondence with the quantum model is accomplished by

$$\nu = \frac{1}{2}(\omega_e - \omega_g)$$

$$R_\uparrow = CEJ^2 \frac{e^{-\beta E}}{1 - e^{-\beta E}}$$

$$R_\downarrow = CEJ^2 \frac{1}{1 - e^{-\beta E}}$$

$$E = \sqrt{A^2 + J^2} \quad (47)$$

The idea of the stochastic approach is that coupling between TLS and chromophore only manifests itself through modulation of the absorption frequency of the chromophore as modulated by TLS hops. TLS dynamics and thermal properties are completely unaffected by the chromophore, hence the total independence of TLS energy scale and flip rates on chromophore properties, that is, these quantities are calculated by setting the TLS−chromophore coupling constant α to zero in our earlier expressions. Of course, it is crucial to keep α in the frequencies, otherwise the TLS would have no effect on the chromophore at all. The stochastic approximation is expected to work quite

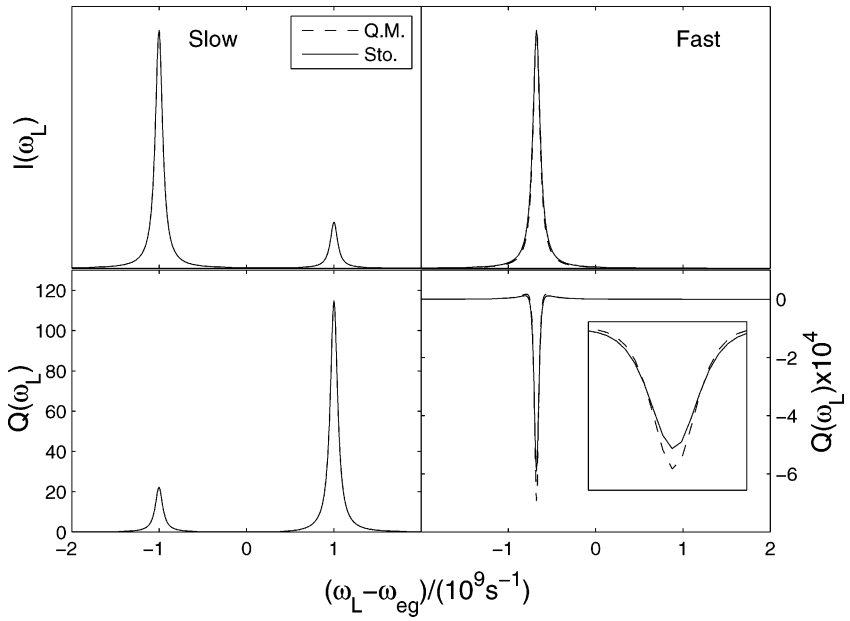

Figure 2. Absorption line shapes and Mandel's Q parameter spectrum in the limit of weak coupling between the chromophore and TLS. Line shapes are presented in arbitrary units. Left and right halves correspond to slow and fast modulations, respectively. Physical parameters used in this calculation include $\Gamma_0 = 100$ M s^{-1}, $\Omega_0 = 1$ M s^{-1}, $T = 1.7$ K, and quantum model parameters taken from ref 55, namely, $A = 2.8$ K, $\alpha = 3.75 \times 10^{11}$ nm^3 s^{-1}, $r = 5.72$ nm, $J = 3 \times 10^{-4}$ K. For the slow modulation, we used $C = 3.9 \times 10^8$ s^{-1} K^{-3}, while for the fast modulation $C = 3.9 \times 10^{18}$ s^{-1} K^{-3}. Within the stochastic approximation, these numbers translate to (eq 47) $\nu = 1.02 \times 10^9$ s^{-1} and $E = 2.8$ K. The upward flip rate $R_\uparrow = 23.5$ s^{-1} for the slow modulation and 2.35×10^{11} s^{-1} for the fast modulation. In the slow modulation, no discrepancy between quantum and stochastic treatments is found. For the fast modulation, the line shape is the same for both quantum and stochastic treatments while in the Q parameter there is a small difference between the models. The inset focuses on this difference.

well when α is small. In that case, transition elements of the Redfield matrix are well approximated by using rates inferred from eq 47. It should be noted that the stochastic approach is obviously deficient in one sense. There are four possible transition frequencies implied by the quantum level diagram in Figure 1, and the stochastic picture only predicts two. For small α and/or large r, half the transitions rarely occur because of poor Franck−Condon overlap. Given our notation, the transitions $c \rightarrow a$ and $d \rightarrow b$ are the strong ones (assuming weak coupling). At high couplings strengths, half of the transitions will necessarily be missed by the stochastic picture. The following numerical examples highlight both the practicality of the present fully quantum approach in calculations as well as the shortcomings of the popular stochastic approximation over certain parameter regimes.

1. Weak Coupling between Chromophore and TLS. "Weak" coupling between the chromophore and TLS is dictated by the condition $A \gg (\alpha/2r^3) = P$. Physically, this can result from either a small coupling constant α or a large distance between the chromophore and TLS. As discussed above, in this case, results of the quantum model and stochastic model should be quite similar (at least for the line shapes[54]). In the left panes of Figure 2, we present the long-time line shape and corresponding Q parameter spectrum for the case of slow TLS modulation and weak TLS−chromophore coupling. The physical constants chosen are detailed in the figure caption and represent realistic numbers for an organic dye molecule embedded in an amorphous host.[55] We compare the quantum model with the associated stochastic approximation. As expected, the line shapes for the two approaches are identical at the resolution of the figure. The two peaks represent the two optical transitions with appreciable overlap ($a \rightarrow c$ and $b \rightarrow d$). The other transitions are so weak as to be invisible at this scale. The difference in peak heights is due to the difference in thermal occupation probabilities for the two TLS states (which are basically unmodified by the chromophore state due to the small value of P in the quantum model). Peak shape is Lorentzian with both line widths given by the spontaneous emission rate (full width at half-maximum is Γ_0). The TLS flipping is so slow in this case that it contributes negligibly to the line widths.

The right panes of Figure 2 display similar information to the left but with parameters chosen to ensure that the TLS flip rate is faster than the difference in transition frequencies, ν. For simplicity, we increased the flip rate by increasing the value of C. While this is physically questionable, it does provide the only direct means to increase the TLS flip rate while leaving all other behavior identical. In this case, the line shape consists of only a single peak due to motional narrowing of the optical transition.[54,56] As in the slow modulation limit, we find quantitative correspondence between stochastic and quantum models for the line shape calculation. The stochastic model does deviate slightly from the quantum result in the calculation of the Q parameter. Though the deviation is slight, it is interesting to note that there are cases where the stochastic model is perfect for line shapes, yet imperfect for higher order statistics. All in all though, for weak coupling, the stochastic approximation is seen to perform well both at slow and fast TLS modulation rates. We note that, in the limiting cases of slow and fast modulation displayed here, the observed spectra can also be predicted on the basis of the physical approximations introduced in ref 39.

2. Strong Coupling between Chromophore and TLS. "Strong" coupling is ensured by the condition $A \sim P = (\alpha/2r^3)$. In this case, the quantum model differs from its associated stochastic approximation in both line shape and Mandel's Q parameter. The left panes of Figure 3 display results for the strong coupling and slow modulation parameter regime of both the quantum and stochastic dynamic treatments. In contrast to our earlier example, strong coupling now implies that transitions between states $d \rightarrow a$ and $c \rightarrow b$ are important and occur with some

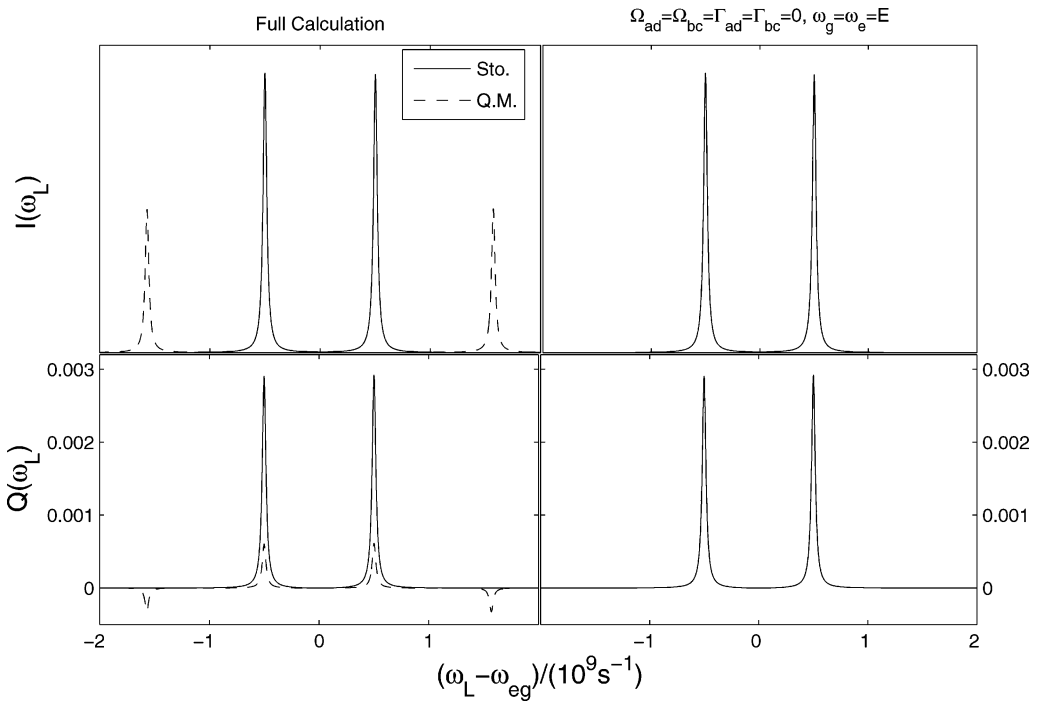

Figure 3. Left panes: the line shape and Mandel's *Q* parameter spectrum for slow TLS modulation with strong coupling between the chromophore and TLS. Due to the strong coupling, $d \rightarrow a$ and $c \rightarrow b$ transitions are significant within a fully quantum framework and result in two additional peaks relative to weak coupling results. The stochastic approach completely misses these additional spectral lines and fares poorly in reproducing the magnitude of peaks in the *Q* spectrum. The plots correspond to the following quantum model parameters: $\Gamma_0 = 40$ M s^{-1}, $\Omega_0 = 0.1$ M s^{-1}, $T = 1.7$ K, $A = 0.006$ K, $J = 0.008$ K, $C = 3.9 \times 10^8$ K^{-3} s^{-1}, $\alpha = 3.75 \times 10^{11}$ nm^3 s^{-1}, and $r = 5.72$ nm. Corresponding stochastic parameters are as follows: $\nu = 501$ M s^{-1}, $E = 0.01$ K, and $R_\uparrow = 42307$ s^{-1}. The right panes display that it is possible to reduce the fully quantum mechanical treatment to the stochastic results by turning off half of the allowed transitions and calculating Redfield elements in a manner consistent with the stochastic approach (see text). In other words, it is relatively simple to trace the failures of stochastic modeling.

finite probability within the fully quantum treatment. Since peak widths are smaller than interpeak spacing, peaks corresponding to all four possible transitions are clearly visible in the quantum mechanical modeling. The relative height of the two central peaks in the line shape are (as in the previous example) related to TLS thermal occupation probabilities. Since $E \ll kT$ for the chosen parameters, both central peaks have effectively the same height. The intensity of the outer two peaks is predicted based on the probability to excite an "off diagonal" transition ($a \rightarrow d$ or $b \rightarrow c$) relative to diagonal transitions. Mathematically, this probability is dictated by the square of the Rabi frequency for the transition in question. Equivalently (see eqs 21 and 22), the ratio of the left two peaks or the right two peaks is predicted to be Γ_{db}/Γ_{da} (1.94 for the case shown), which agrees with the numerical results. It is obvious that the stochastic approximation predicts a very different line shape and *Q* parameter since it does not account for the transitions $d \rightarrow a$ and $c \rightarrow b$. While one could argue that the stochastic model does do a good job in predicting that portion of the absorption line shape which it is capable of reproducing (the center two peaks), even the center two peaks are clearly off in magnitude for the *Q* parameter. The stochastic model fares very poorly in this parameter regime (strong coupling, slow modulation).

The failure of the stochastic model in this case was predictable, and we can trace its origins back to failures to reproduce the full system dynamics in a realistic manner. The right panes of Figure 3 are meant to display that we understand exactly where these failures are coming from. These panes actually display two different cases (although they overlap so only a single line is visible): the stochastic calculation from the left panes and a modified quantum calculation where the evolution operator was altered such that all nondiagonal transitions were turned off ($\Omega_{ad} = \Omega_{bc} = \Gamma_{ad} = \Gamma_{bc} = 0$ and $\Omega_{ac} = \Omega_{bd} = \Omega_0$ and $\Gamma_{ac} = \Gamma_{bd} = \Gamma_0$) and all Redfield elements were calculated assuming that $\omega_g = \omega_e = E$. While these two changes do not fully reduce the quantum calculation to the stochastic treatment from a mathematical standpoint, the physical basis is clear. The alterations explicitly remove the nondiagonal transitions that the stochastic model necessarily misses, and it evaluates the TLS jump rates in the same approximation inherent to the stochastic approach. There are more subtle effects within the Redfield treatment (as in the evolution of coherences) so that our ad hoc alterations do not fully limit to a stochastic model, however these effects clearly do not contribute to the line shape and *Q* spectrum calculations. The primary problem with a stochastic model in predicting photon counting observables is in the loss of "off-diagonal" nuclear transitions and incorrect estimation of relaxation rates.

In Figure 4, we show two cases of reasonably fast modulation speed and strong coupling; the difference between the left and right panes is quantitative (see the figure axes for *Q*) and is intended to display the fact that one can tune the *Q* parameter by adjusting field strengths. For a simple (no coupling to a bath) two-level chromophore, antibunching is maximized when excitation and emission rates are equalized[57] and a qualitatively similar effect is seen here. Although both quantum and stochastic models will eventually narrow into a single peak for high enough flip rates, it is interesting to see in this intermediate regime that the stochastic model has already narrowed, while the quantum picture retains a more complex structure. This structure is visible in both the line shape and *Q* parameter calculations.

3. Emission Spectra. In Figure 5, we display emission line shapes and Mandel's *Q* parameter spectra for the same physical parameters selected in Figure 3 (except the Rabi frequency, which was set to provide relatively large magnitudes of the *Q* parameter in the antibunching regimes). As discussed previously,

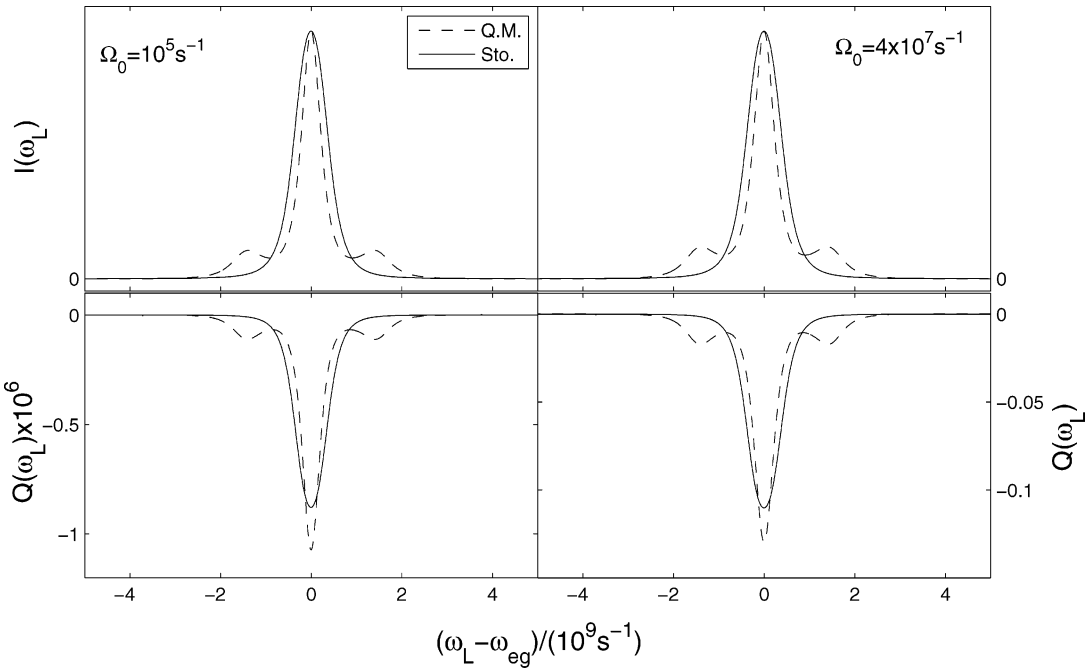

Figure 4. Line shape and Mandel's *Q* parameter for intermediate TLS modulation rate, with "strong" coupling between the chromophore and TLS. The quantum model parameters are the same as those in Figure 3 except for the coupling constant which is modified to $C = 3.9 \times 10^{12}$ K^{-3} s^{-1}, corresponding to upward flip rate $R_{\uparrow} = 4.23 \times 10^{8}$ s^{-1} in the stochastic model. In the left panes, the Rabi frequency coefficient is $\Omega_0 = 10^5$ s^{-1}, while in the right panes $\Omega_0 = \Gamma_0 = 40$ M s^{-1}. Comparison of the left and right panes shows that antibunching increases as excitation and emission rates become comparable.

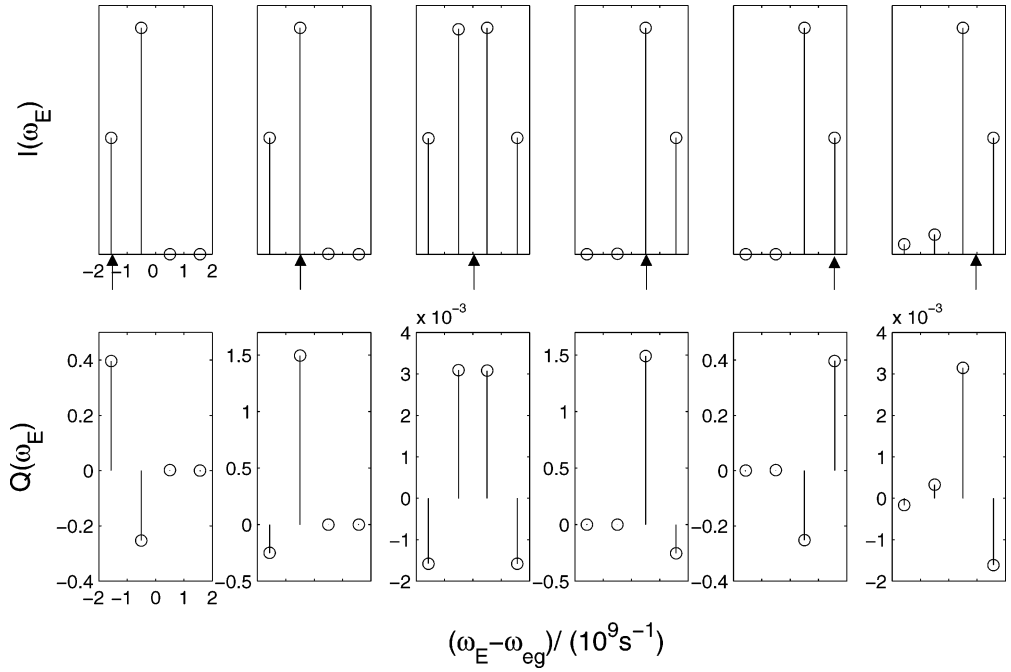

Figure 5. Emission line shapes and Mandel's parameter *Q* for slow modulation limit with "strong" coupling between the chromophore and TLS. The excitation laser frequencies are marked in the figure using "↑". The excitation frequencies, from left to right, are $\omega_{eg} + \omega_{cb}$, $\omega_{eg} + \omega_{ca}$, ω_{eg}, $\omega_{eg} + \omega_{db}$, $\omega_{eg} + \omega_{da}$, and $\omega_{eg} + 0.6\omega_{da}$ (see Figure 1). The spontaneous emission rate and the Rabi frequency are $\Gamma_0 = 40$ M s^{-1} and $\Omega_0 = 4$ M s^{-1}, respectively. The quantum model parameters are as follows: $T = 1.7$ K, $A = 0.006$ K, $J = 0.008$ K, $\alpha = 3.75 \times 10^{11}$ nm^{-3} s^{-1}, $C = 3.9 \times 10^{8}$ K^{-3} s^{-1}, and $r = 5.72$ nm.

our simulation methodology does not allow for true calculation of emission spectra. The frequency dependence we obtain is resolved solely on the basis of individual state-to-state transitions—we assign all photons emitted for a given transition the resonance frequency of that transition. Hence, the "line shapes" in Figure 5 are not broadened by the radiative lifetime of the chromophore or by any other source and line shifts are not captured. Physically, the spectra we obtain would match an experimental measurement with an instrument unable to resolve frequency differences less than the radiative line width.

The multiple panels in both rows of Figure 5 reflect different laser exciting frequencies. Four different resonant excitations corresponding to all possible transitions and two off resonant frequencies are considered. Clearly, there is a strong dependence in the emission spectra on the exciting frequency. This is expected since TLS dynamics are slow enough in this problem

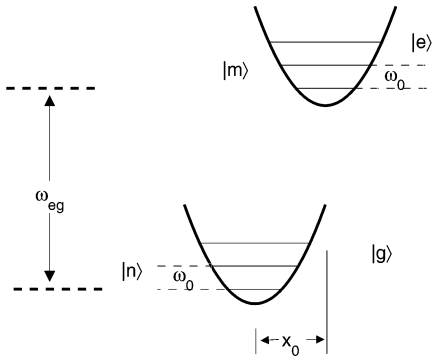

Figure 6. Schematic description of a system with two electronic levels and single harmonic vibrational mode.

that the TLS does typically not have a chance to relax to equilibrium while the chromophore is excited. Resonant excitation to state *c*, regardless of which ground state (*a* or *b*) the transition starts from, results in the same emission line shape (left two panes of the top row of Figure 5). The relative peak heights simply reflect Condon overlaps in the spontaneous emission process from state *c* back to *a* or *b*. These overlaps do not care how state *c* was excited and generate identical emission spectra regardless of which resonant transition is excited. Similar arguments explain the right three panes of the top row of Figure 5. All three excitation frequencies result in the occupation of state *d*, and the emission line shapes are insensitive to details of the excitation beyond this fact—even when the excitation is off resonance with either $a \rightarrow d$ or $b \rightarrow d$ transitions. When an off resonant excitation is considered that has equal probability to excite to either *c* or *d*, the emission line shapes reflect a symmetric combination of the previously discussed cases (third pane of the top row of the figure).

In contrast to the line shapes, *Q* parameter spectra are highly sensitive to excitation frequency (bottom row of Figure 5). The basis for this effect is quite simple. When photons are counted at the same frequency of the exciting laser, we expect to see photon bunching. For example, looking at the leftmost peak in the leftmost pane of the bottom row, we excite $b \rightarrow c$ transitions and monitor $c \rightarrow b$ emissions. Photons are repeatedly ejected as this cycle repeats until spontaneous emission induces a $c \rightarrow a$ transition (or the TLS flips), at which point the system is off resonance and has to wait for a TLS flip to return the system to the excitable state *b*. The interspersion of bright and dark intervals leads to bunching phenomena and a positive *Q* parameter. In contrast, when excitation does not correspond to the monitored transition (second peak from left in the leftmost pane), a three-state cycle repeatedly occurs ($b \rightarrow c \rightarrow a \rightarrow b$ ... or a similar variant) as photons are detected. There is no jumping between periods of "bright" or "dark" since the pathway for repeated photon emission necessarily involves both TLS and radiative/excitation dynamics. The chosen time scales in this example ensure that no single rate is limiting over all others in this cycling process and antibunching results (if a single time scale were completely dominant, we would expect $Q = 0$). Similar arguments can be applied to the remaining panes of the *Q* parameter spectrum. This example makes a clear case for measurement of higher order photon counting moments. Different aspects of system dynamics are captured in the measurement of the *Q* parameter beyond what is seen in simple line shape statistics. Furthermore, examination of the emission statistics provides a more detailed measure than possible solely on the basis of absorption statistics.

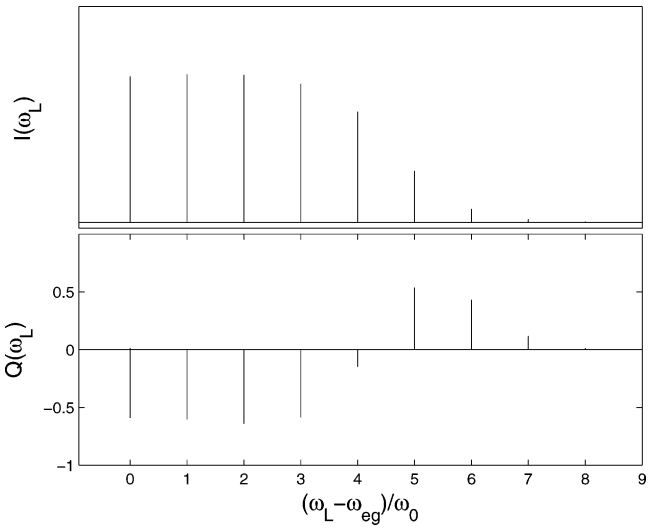

Figure 7. Line shape and Mandel's *Q* parameter spectrum as a function of exciting laser frequency for a chromophore with a harmonic vibrational coordinate. The spontaneous emission rate and Rabi frequency are $\Gamma_0 = \Omega_0 = 10^8\ s^{-1}$ and the coupling strength is $R_0 = 10^7\ s^{-1}$. Physical parameters specific to the chromophore are detailed in the text.

IV. Chromophore With Nuclear Vibrations Coupled To A Harmonic Bath

A. Model Description. As a more complex example of multilevel quantum dynamics, we consider the case of a chromophore with a harmonic vibrational degree of freedom. Coupled to this vibrational coordinate is a bath modeled by an ensemble of harmonic oscillators. Such models are standard in the treatment of molecular spectroscopy[47] but have seen little prior use in the treatment of photon statistics. Within the Born−Oppenheimer approximation, the Hamiltonians of the chromophore in its electronic ground, $|g\rangle$, and excited, $|e\rangle$, states are taken to be

$$H_g = \frac{1}{2}\hbar\omega_0[P^2 + X^2] \tag{48}$$

$$H_e = \hbar\omega_{eg} + \frac{1}{2}\hbar\omega_0[P^2 + (X - X_0)^2]$$

where *X* and *P* are related to the nuclear position coordinate *x* and momentum *p* by

$$X = \sqrt{\frac{m\omega_0}{\hbar}}\,x$$

$$P = \frac{1}{\sqrt{m\omega_0\hbar}}\,p \tag{49}$$

The vibrational coordinate thus has frequency ω_0 and $\hbar\omega_{eg}$ is the excitation energy for the 0−0 transition. x_0 is the shift in equilibrium position of the nuclear coordinate between excited and ground states (see Figure 6). The interaction with the thermal bath is assumed to be linear in both *X* and bath coordinates X_i, that is

$$V = CX\sum_j X_j \tag{50}$$

where *C* is a constant specifying the interaction strength between system and bath. The harmonic bath Hamiltonian is

$$H_B = \sum_j \frac{1}{2}\hbar\omega_j(P_j^2 + X_j^2). \tag{51}$$

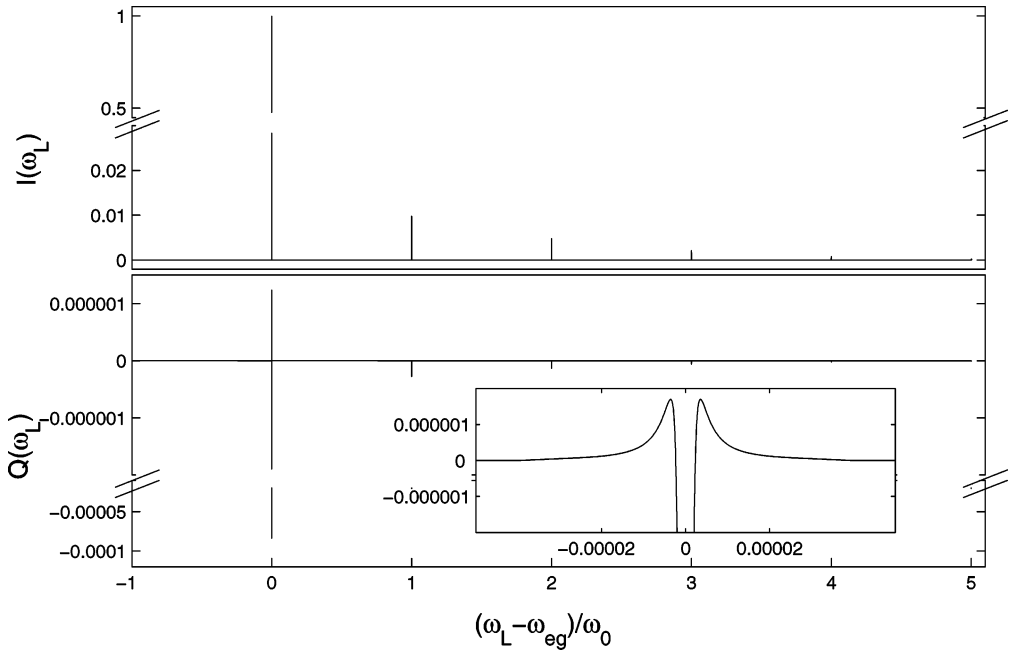

Figure 8. Similar to Figure 7, but with $R_0 = 10^{10}$ s^{-1}, $\Gamma_0 = 10^8$ s^{-1}, and $\Omega_0 = 10^6$ s^{-1}. This system is in the linear response regime. The inset shows the variation of Q in the vicinity of $\omega_L = \omega_{eg}$.

The above definitions of H_g, H_e, V, and H_B provide all necessary information to proceed directly with the calculation of $\mathbb{L}$ and related quantities as detailed in section II. We make a few brief comments related to the calculation of Redfield elements below to clarify our notation. More detailed presentations can be found elsewhere.[47,48,58]

The linear interaction between bath and system is only capable of effecting transitions between adjacent vibrational states in the same electronic manifold, that is, $|n\rangle \rightarrow |n+1\rangle$ or $|n\rangle \rightarrow |n-1\rangle$. This is seen, by introducing the usual creation and annihilation operators ($a = (X + iP)/(2)^{1/2}$, $a^\dagger = (X - iP)/(2)^{1/2}$) to write the interaction matrix elements between excited-state levels in the form

$$V_{n_e,n'_e} = \frac{1}{2} C[\sqrt{n'_e}\,\delta_{n_e,n'_e-1} + \sqrt{n_e}\,\delta_{n_e,n'_e+1}] \sum_j (a_j + a_j^\dagger) \quad (52)$$

and similarly for the ground state. The creation and annihilation operators only allow for adjacent transitions as indicated by the above delta functions. The bath properties

$$a_j(t) = e^{-i\omega_j t} a_j(0)$$

$$a_j^\dagger(t) = e^{i\omega_j t} a_j^\dagger(0)$$

$$\langle a_j a_j^\dagger \rangle_b = (1 - e^{-\beta\hbar\omega_j})^{-1}$$

$$\langle a_j^\dagger a_j \rangle_b = e^{-\beta\hbar\omega_j}(1 - e^{-\beta\hbar\omega_j})^{-1} \quad (53)$$

are used to evaluate all correlation functions associated with the Redfield matrix calculation. In this model, the interaction matrix V is explicitly real leading to a slightly simplified calculation for the Redfield matrix

$$\mathbb{R}_{mnpq} = t_{pmnq} + t_{qnmp} - \delta_{mp} \sum_r t_{nrrq} - \delta_{nq} \sum_r t_{mrrp} \quad (54)$$

where

$$t_{pmnq} = \frac{1}{2\hbar^2} \int_{-\infty}^{\infty} d\tau e^{i\omega_{qn}\tau} \langle \hat{V}_{pm}(\tau) \hat{V}_{nq}(0) \rangle_b \quad (55)$$

t_{pmnq} is nonzero only if both of the pairs (p,m) and (n,q) involve states in the same electronic manifold. The integration can be carried out and yields

$$t_{pmnq} = R_0 [\sqrt{m}\,\delta_{p,m-1} + \sqrt{p}\,\delta_{p,m+1}] [\sqrt{n}\,\delta_{q,n-1} + \sqrt{q}\,\delta_{q,n+1}] \sum_j \frac{\delta(\omega_j + \omega_{qn}) + e^{-\beta\hbar\omega_j}\delta(\omega_j - \omega_{qn})}{1 - e^{-\beta\hbar\omega_j}} \quad (56)$$

Unlike the TLS model, in this case, every allowable ω_{qn} is exactly the same and is equal to ω_0. This is due to the equality of spacing between levels in the harmonic oscillator model and the form of V which only allows for adjacent transitions. Thus, the density of bath states is not important in calculating the Redfield matrix elements in this case and only a single constant R_0 enters into the Redfield description as a measure of coupling between system and bath. For example, elements of the form $\mathbb{R}_{nn;n+1n+1}$ are given in our notation by

$$\mathbb{R}_{nn;n+1n+1} = 2R_0(n+1)(1 - e^{-\beta\hbar\omega_0})^{-1} \quad (57)$$

Since this element reflects the rate of transition from harmonic oscillator state $|n+1\rangle$ to $|n\rangle$, it is clear that R_0 is closely related to the relaxation rate of our vibrational coordinate.

B. Numerical Results. In the following calculations, we choose physical parameters specifying the chromophore to be $\omega_0 = 3.77 \times 10^{13}$ s^{-1}, $x_0 = 0.11$ Å, $m = 10^5\ m_e$ (m_e is the electron mass), and $T = 10$ K. (The energy difference between neighboring levels of the harmonic oscillator $\hbar\omega_0$ corresponds to a temperature of 287.75 K.) While these numbers are suggestive of a heavy diatomic molecule (like I_2) in a low-temperature matrix, we have not made a serious attempt to connect these calculations with physical systems. Rather, we

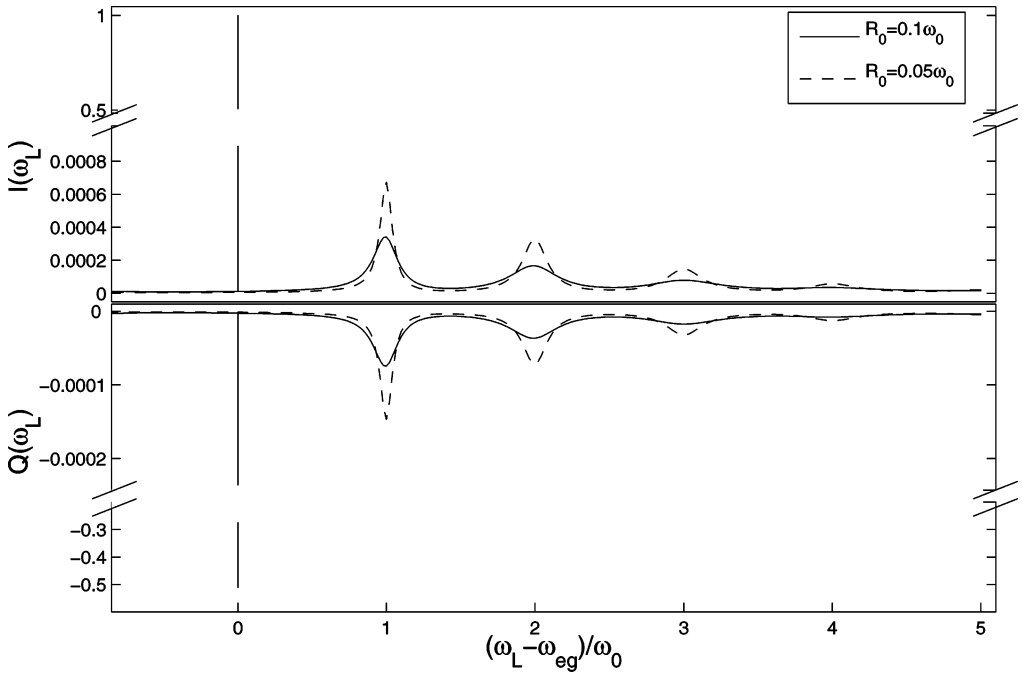

Figure 9. Similar to Figure 7, but with $\Gamma_0 = \Omega_0 = 10^9\ s^{-1}$ and $R_0 = 0.1\omega_0$ (solid line) and $R_0 = 0.05\omega_0$ (dashed line). Note that in this case the width of the peak at 0 is much smaller than the width of the other peaks, since it does not depend on R_0. Peak widths are given by the nonradiative lifetime of the various states for all other transitions.

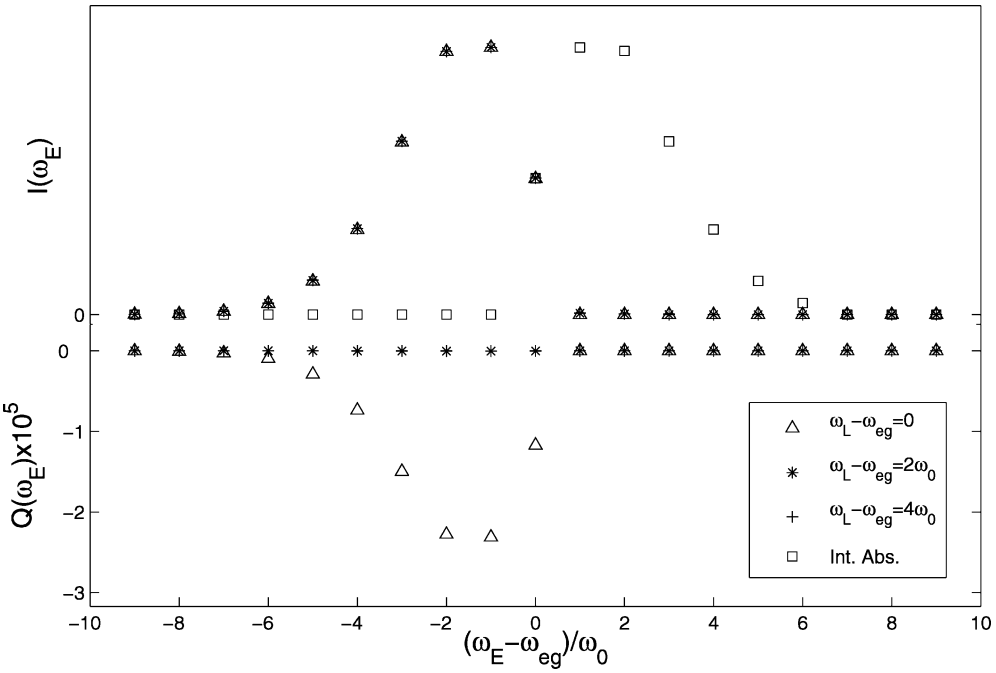

Figure 10. Emission line shape and emission *Q* spectrum for parameters reflecting the linear response regime. Three different excitation frequencies are considered as noted in the legend. The chosen physical parameters parallel those of Figure 8. Since the system behaves in accord with linear response, the emission line shapes are the same for all excitation frequencies and also in agreement (mirror image) with the integrated absorption spectrum.

have chosen x_0 to provide Condon overlaps that are close to vertical, while still ensuring finite probability for transitions up to 0−6. We have also set the temperature somewhat arbitrarily while we will freely adjust R_0 in the following examples to meet our needs in displaying various phenomena. The Redfield approach we employ is necessarily limited to a finite number of states due to numerical considerations. We cannot solve the equations for $N = \infty$. In the numerics presented here, we used 10 levels in each of the electronic states ($n = 0$ to $n = 9$). It was verified that altering the number of vibrational states to include more levels did not change any results at the resolution of the presented figures. We note that the size of $\mathbb{L}$ for these calculations is 400 × 400. Using the methods of section IIC requires only diagonalization of this matrix, which is a simple task for modern computers.

1. Weak Coupling between System and Bath (R_0 small) Case. The case of weak coupling corresponds to slow vibrational relaxation. In Figure 7, we show the line shape and the *Q* parameter for a case in which the relaxation rate is slower than all other rates in the problem including the spontaneous emission rate, Rabi frequency, and oscillator frequency. This leads to nonthermal distributions of vibrational levels within both elec-

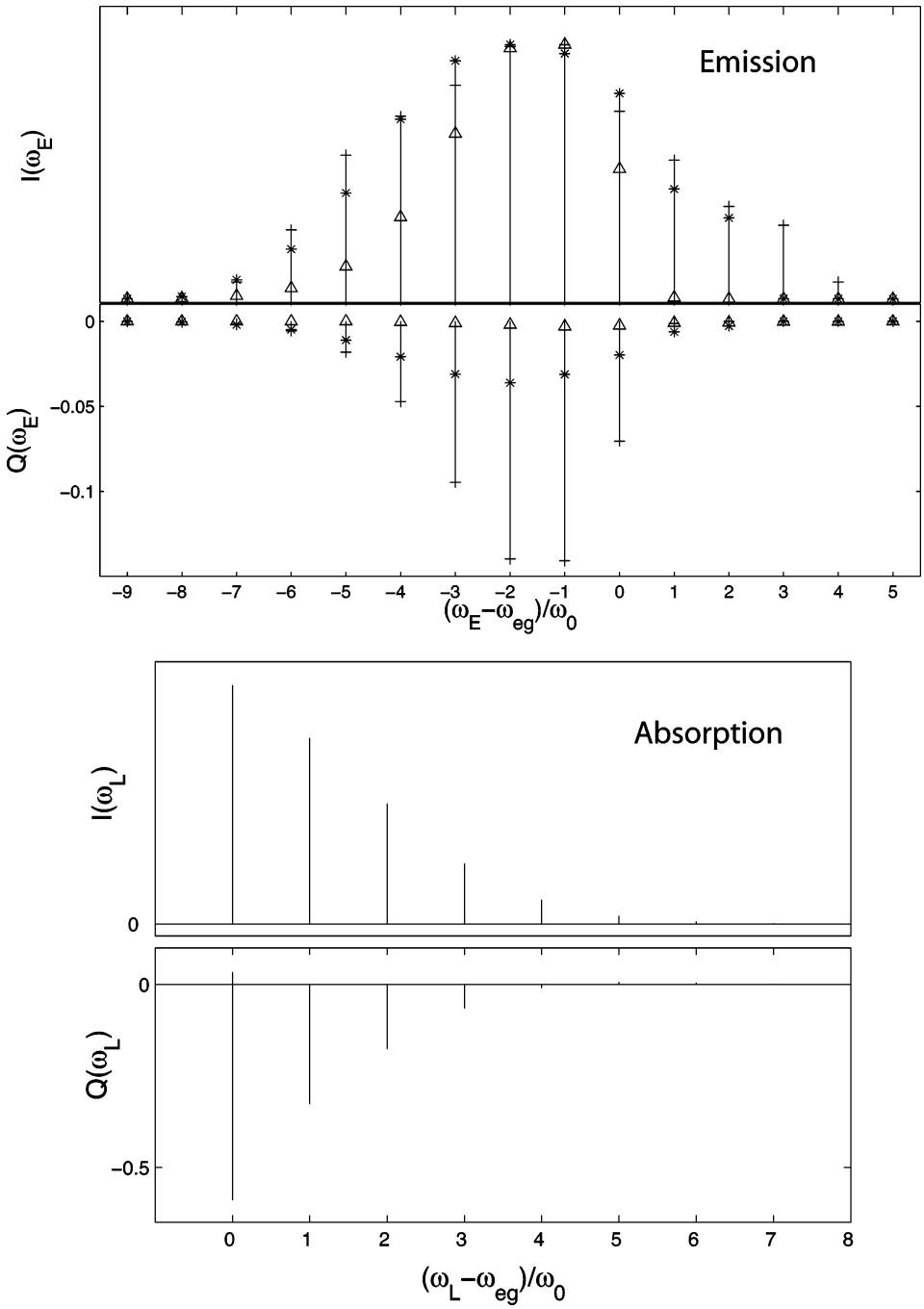

Figure 11. Emission line shape and Q spectrum for parameters outside the linear response limit: $R_0 = \Gamma_0 = \Omega_0 = 10^8\ s^{-1}$. The exciting fields are the same as those in Figure 10. In this case, the linear response approximation is not valid anymore and both the line shape and Q spectra differ with excitation frequency. The absorption line shape was calculated with the same parameters and is included for comparison purposes.

tronic manifolds at steady state since the system is unable to fully relax between subsequent photon emission/absorption events. Interestingly, the variation of these steady states with excitation frequency and the variation of Condon overlaps between the various transitions leads to Q parameter values spanning a range of positive and negative values depending on the excitation frequency. It should be noted that, although the spectra appear to have only been evaluated at the various allowed resonance frequencies, this is not the case. It is simply the case that the radiative line widths are much narrower than discernible at the resolution of the figure.

Figure 8 shows the line shape and Q parameter for a case in which the relaxation is slow relative to the harmonic oscillation frequency ω_0 but is faster than the spontaneous emission rate and the Rabi frequency. In this case, the relative amount of power absorbed by each possible transition is expected to agree with linear response predictions since the vibrational state of the chromophore should almost always be in the relaxed ($n = 0$) state without significant perturbation by the relatively weak coupling to the field. Linear response theory predicts that the strength of each transition is due to the Condon overlap between $n = 0$ in the ground state (remember $kT \ll \hbar\omega_0$ in this model) and the various excited states. The displayed line shapes appear to contradict this prediction, most clearly due to the very tall zero phonon peak at $\omega_L = \omega_{eg}$ relative to the other peaks. However, the height of this line is due to the fact that this transition is not broadened by nonradiative processes as are the remaining transitions. The line width of the 0−0 line is approximately

equal to Γ_0 whereas the other widths are dominated by nonradiative decay on the order of R_0 and are 100 times wider. The relevant quantities to compare with linear response results are the intensities of each transition integrated over the local vicinity of the transition. In Figure 10, we display such integrated absorption peaks alongside emission lines (discussed below). These integrated lines show perfect agreement with linear response results with relative intensities directly proportional to the square of nuclear overlap.

One interesting point to note about the Q parameter in these calculations is that it undergoes rapid variation with excitation frequency in the vicinity of the 0−0 line. While this behavior does not seem amenable to simple explanation, it has been observed previously in simpler models both numerically[38] and analytically.[42] It should also be emphasized that the magnitude of Q is largely due to the ratio between Γ_0 and Ω_0 as seen in Figure 4. Here, this ratio is large, leading to small negative Q values. Smaller ratios lead to larger magnitudes of Q (when Q is negative).

2. Strong Coupling between the System Bath (R_0 not small) Case. An example of fast relaxation, with R_0 on the order of ω_0, is shown in Figure 9. In this case, the width of the peaks is of the same order as the distance between the peaks and line shape is clearly not a series of thin sticks as in previous examples. Note that since the peak at $\omega_L = \omega_{eg}$ does not involve any thermal relaxation it is independent of R_0. The width of this peak is still specified by the spontaneous emission rate, which is orders of magnitude lower than the remaining peak widths (on the order of R_0) leading to its very large height. In this plot, we have chosen identical values for Γ_0 and Ω_0, which leads to sizable negative Q values for the 0−0 line.

3. Emission Spectroscopy. In Figure 10, we show the emission line shape and Q parameter spectra for parameters appropriate to the linear response regime (identical parameters to Figure 8). It is shown that in this case the line shape is the same for all excitation frequencies (in the figure we show $\omega_L - \omega_{eg} = 0$, $2\omega_0$, $4\omega_0$). It is also shown that integration of the absorption spectrum over the individual transition line widths provides a mirror image of the emission line shape as expected in the linear response regime. Recall that our emission line shapes are sensitive only to individual transitions, so the emission spectra are automatically of the "integrated" type and comparison between emission and integrated absorption is completely natural. While emission line shapes are insensitive to excitation frequency in this regime, the Q parameter exhibits strong dependence on excitation frequency.

Figure 11 shows the emission line shape and Q parameter for stronger driving fields and slower relaxation rates than those present in Figure 10. The system is no longer in the linear response regime, and line shapes differ for different excitation frequencies. The parameters were chosen to equalize all relevant physical time scales, demonstrating that there is no simple relationship possible between excitation frequency, emission line shape, and emission Q parameter in general.

V. Conclusion

We have introduced a practical framework for the calculation of photon counting statistics in quantum systems with multiple levels and dissipative coupling to a thermal environment. The present scheme generalizes previous work by extending the treatment of chromophore dynamics beyond the stochastic models historically applied to single molecule spectroscopy. Our model calculations for TLS dynamics explicitly demonstrate some of the failings of traditional stochastic modeling (especially in the case of strong coupling to the environment). In the case of harmonic vibrations, use of a stochastic model is even more suspect since all quantization of the vibrational coordinate will be lost. Although one could envision more elaborate kinetic schemes in an attempt to model these systems, it seems more straightforward to simply treat the dynamics correctly, quantum mechanically, from the outset. The methods presented here provide a prescription to do this.

We acknowledge that there is an unfortunate amount of machinery behind the calculations that we have presented here, however it is important to stress that the majority of this overhead is associated with implementation of the Redfield formalism (calculation of the matrix $\mathbb{L}$ in our notation). Equation 40 is very easily applied once $\mathbb{L}$ is given—simply diagonalize the matrix and perform a few simple matrix multiplications as implied by the formulas. The generating function approach, while necessarily encumbered by the usual difficulties in simulating dissipative quantum systems, adds no new significant conceptual or numerical problems. Photon counting statistics are therefore readily available at no more expense than normally expected for calculation of density matrix dynamics. This remarkable fact seems to be the strongest point in support of the generating function methodology.

Several of our calculations have presented results for emission spectra and the corresponding Q parameter quantities. Although such measurements are not yet within the capabilities of experiment, we believe that a strong case can be made for the development of single molecule detectors with spectral resolution. It is clear from our model calculations that emission spectroscopy provides a different and (when combined with absorption spectroscopy) more revealing signature of chromophore dynamics than obtainable from absorption alone. This is not surprising, but the present study is (to our knowledge) the first to demonstrate this fact explicitly. As we have repeatedly stated, the present scheme for emission spectroscopy is sensitive only to molecular transitions and not directly to emission frequency. Emission frequency is assumed to be on resonance with specific transitions. While this approach works well in the limit of weak coupling to the environment, stronger coupling invariably leads to level shifts, motional narrowing as associated complications. A general and practical formulation of true emission photon counting statistics has yet to be developed.

Acknowledgment. F.B. dedicates this paper to his graduate advisor, Bob Silbey. Without Bob I would not know the first thing about single molecule spectroscopy, Redfield dynamics, or line shape theory. Thank you for your mentorship and guidance over the years. This research was supported in part by the Research Corporation and the National Science Foundation (CHE-0349196, CHE-0321368). F.B. is an Alfred P. Sloan Research Fellow.

References and Notes

(1) Moerner, W. E.; Kador, L. *Phys. Rev. Lett.* **1989**, *62*, 2535−2538.
(2) Orrit, M.; Bernard, J. *Phys. Rev. Lett.* **1990**, *65*, 2716−2719.
(3) Moerner, W. E.; Orrit, M. *Science* **1999**, *283*, 1670−1676.
(4) Plakhotnik, T.; Donley, E. A.; Wild, U. P. *Annu. Rev. Phys. Chem.* **1997**, *49*, 181−212.
(5) Lu, H. P.; Xun, L.; Xie, X. S. *Science* **1998**, *282*, 1877−1882.
(6) Xie, X. S. *J. Chem. Phys.* **2002**, *117*, 11024−11032.
(7) Zhuang, X.; Bartley, L. E.; Babcock, H. P.; Russell, R.; Ha, T.; Herschlag, D.; Chu, S. *Science* **2000**, *288*, 2048−2051.
(8) Weiss, S. *Science* **1999**, *283*, 1676−1683.
(9) Jung, Y.; Barkai, E.; Silbey, R. J. *J. Chem. Phys.* **2002**, *117*, 10980−10995.
(10) Orrit, M. *J. Chem. Phys.* **2002**, *117*, 10938−10946.
(11) Bohmer, M.; Enderlein, J. *ChemPhysChem* **2003**, *4*, 793−808.

(12) Lippitz, M.; Kulzer, F.; Orrit, M. *ChemPhysChem* **2005**, *6*, 770−789.
(13) Jung, Y.; Barkai, E.; Silbey, R. J. *J. Chem. Phys.* **2002**, *117*, 10980−10995.
(14) Geva, E.; Skinner, J. L. *J. Phys. Chem. B* **1997**, *44*, 8920−8932.
(15) Wang, J.; Wolynes, P. *Phys. Rev. Lett.* **1995**, *74*, 4317−4320.
(16) Wang, J.; Wolynes, P. *J. Chem. Phys.* **1999**, *110*, 4812−4819.
(17) Schenter, G. K.; Lu, H. P.; Xie, X. S. *J. Phys. Chem. A* **1999**, *103*, 10477−10488.
(18) Portman, J. J.; Wolynes, P. G. *J. Phys. Chem. A* **1999**, *103*, 10602−10610.
(19) Agmon, N. *J. Phys. Chem.* **2000**, *104*, 7830−7834.
(20) Cao, J. *Chem. Phys. Lett.* **2000**, *327*, 38−44.
(21) Yang, S.; Cao, J. *J. Phys. Chem. B* **2001**, *105*, 6536−6549.
(22) Barsegov, V.; Chernyak, V.; Mukamel, S. *J. Chem. Phys.* **2002**, *116*, 4240−4251.
(23) Barsegov, V.; Mukamel, S. *J. of Phys. Chem. A* **2004**, *108*, 15−24.
(24) Barkai, E.; Jung, Y.; Silbey, R. *Phys. Rev. Lett.* **2001**, *87*, Art. No. 207403.
(25) Jung, Y.; Barkai, E.; Silbey, R. *Chem. Phys.* **2002**, *284*, 181−194.
(26) Brown, F. L. H. *Phys. Rev. Lett.* **2003**, *90*, Art. No. 028302.
(27) Fleury, L.; Segura, J.-M.; G. Zumofen, B. H.; Wild, U. P. *Phys. Rev. Lett.* **2000**, *84*, 1148−1151.
(28) Gopich, I. V.; Szabo, A. *J. Chem. Phys.* **2003**, *118*, 454−455.
(29) Gopich, I. V.; Szabo, A. *J. Chem. Phys.* **2005**, *122*, Art. No. 014707.
(30) Flomenbom, O.; Klafter, J.; Szabo, A. *Biophys. J.* **2005**, *88*, 3780−3783.
(31) Plenio, M. B.; Knight, P. L. *Rev. Mod. Phys.* **1998**, *70*, 101−144.
(32) Makarov, D. E.; Metiu, H. *J. Chem. Phys.* **2001**, *115*, 5989−5993.
(33) Osad'ko, I. S. *JETP* **1998**, *86*, 875−887.
(34) Verberk, R.; Orrit, M. *J. Chem. Phys.* **2003**, *119*, 2214−2222.
(35) Jung, Y.; Barkai, E.; Silbey, R. J. *Adv. Chem. Phys.* **2002**, *123*, 199−266.
(36) Zheng, Y.; Brown, F. L. H. *Phys. Rev. Lett.* **2003**, *90*, Art. No. 238305.
(37) Zheng, Y.; Brown, F. L. H. *J. Chem. Phys.* **2003**, *119*, 11814−11828.
(38) Zheng, Y.; Brown, F. L. H. *J. Chem. Phys.* **2004**, *121*, 3238−3252.
(39) Zheng, Y.; Brown, F. L. H. *J. Chem. Phys.* **2004**, *121*, 7914−7925.
(40) Cook, R. J. *Phys. Rev. A* **1981**, *23*, 1243−1250.
(41) Mukamel, S. *Phys. Rev. A* **2003**, *68*, Art. No. 063821.
(42) He, Y.; Barkai, E. *Phys. Rev. Lett.* **2004**, *93*, Art. No. 068302.
(43) He, Y.; Barkai, E. *J. Chem. Phys.* **2005**, *122*, Art. No. 184703.
(44) Sanda, F.; Mukamel, S. *Phys. Rev. A* **2005**, *71*, Art. No. 033807.
(45) Loudon, R. *The Quantum Theory of Light*, 3rd ed.; Oxford: New York, 2000.
(46) Cohen-Tannoudji, C.; Dupont-Roc, J.; Grynberg, G. *Atom-Photon Interactions*; Wiley-Interscience: New York, 1992.
(47) Mukamel, S. *Principles of Nonlinear Optical Spectroscopy*; Oxford: New York, 1995.
(48) Blum, K. *Density Matrix Theory and Applications*, 2nd ed.; Plenum Press: New York, 1981.
(49) Schatz, G.; Ratner, M. *Quantum Mechanics in Chemistry*; Prentice Hall: Englewood Cliffs, NJ, 1993.
(50) van Kampen, N. G. *Stochastic Processes in Physics and Chemistry*; North-Holland: Amsterdam, The Netherlands, 1992.
(51) Mandel, L. *Opt. Lett.* **1979**, *4*, 205−207.
(52) Phillips, W. A. *J. Low Temp. Phys.* **1972**, *7*, 351.
(53) Anderson, P. W.; Halperin, B. I.; Varma, C. M. *Philos. Mag.* **1972**, *25*, 1−9.
(54) Silbey, R. Relaxation theory applied to scattering of excitations and optical transitions in crystals and solids. In *Relaxation Processes in Molecular Excited States*; Funfschilling, J., Ed.; Kluwer Academic Publishers: Boston, MA, 1989.
(55) Brown, F. L. H.; Silbey, R. J. *J. Chem. Phys.* **1998**, *108*, 7434−7450.
(56) Kubo, R. A stochastic theory of line-shape and relaxation. In *Fluctuation, Relaxation and Resonance in Magnetic Systems*; TerHaar, D., Ed.; Oliver and Boyd: Edinburgh, U.K., 1962.
(57) Brown, F. L. H. *Acc. Chem. Res.* **2006**, *39*, 363−373.
(58) Pollard, W. T.; Friesner, R. A. *J. Chem. Phys.* **1994**, *100*, 5054−5065.